Motions of a Rimless Spoked Wheel: a Simple 2D System with Impacts

Michael J. Coleman and Andy Ruina
Department of Theoretical and Applied Mechanics
Cornell University, Ithaca, NY 14853-7501 USA

To be submitted for publication in *Dynamics and Stability of Systems*

Draft August 22, 2001, revised August 19, 2002

Abstract

We discuss the dynamics and stability of a rigid rimless spoked wheel, or regular polygon with an axisymmetric mass distribution, confined to 'rolling' in a vertical plane up or down a slope. By *rolling*, we mean motions in which the wheel hinges on one 'support' spoke until another spoke collides with the ground, followed by transfer of support to that spoke, and so on. Motions are smooth and energy conserving except at instants of spoke collision. It is the simplest of the passive-dynamic mechanical analogues to two-legged walking; it has neither actuation nor control yet exhibits asymptotically stable periodic motions. We derive a return map for the full nonlinear system and find it has two coexisting fixed points corresponding to (1) standing still on two spokes and (2) limit cycle motion. The fixed points are asymptotically stable for all parameters. The fixed points' existence depends on slope angle; for very small slope angles only standing still exists, for intermediate angles both fixed points exist, and for large angles, only limit cycles exist. For intermediate slope angles, we find the basins of attraction for each fixed point. In the limit as the number of spokes goes to infinity, we show that the behavior of the rimless wheel approaches that of a disk rolling without slip or dissipation on a flat surface. This work is a prequel to [M. J. Coleman, A. Chatterjee, and A. Ruina, *Dynamics and Stability of Systems*, 12(3), (Sept., 1997)] in which the authors show that the rimless wheel's 2D limit cycle has 3D asymptotic stability as well.

1 Introduction

In his studies of legged locomotion, McGeer[4, 5, 6, 7, 8], claiming to follow Margaria[3], carried out a stability analysis of a rimless spoked wheel (or, alternatively, it could be a polygonal wheel) confined to move in a vertical plane in a fixed direction down a slope. Figure 1 shows the configuration and parameters for the wheel.

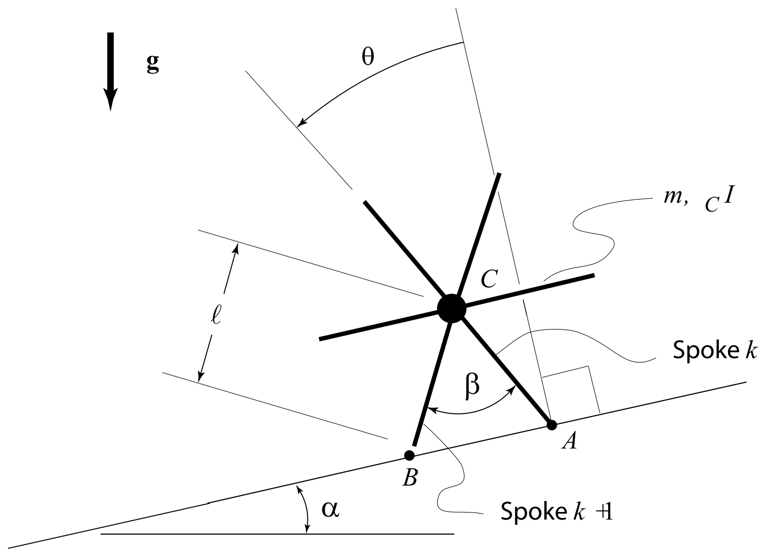

Figure 1: Wheel model: a rimless spoked wheel of mass m, moment of inertia about the center of mass I_C, and n evenly spaced identical spokes of length l rolls down a slope of angle α. The orientation of the wheel is given by angle θ. The angle between the spokes is $\beta = 2\pi/n$.

This 2D rimless wheel was McGeer's starting point in an evolution of increasingly anthropomorphic yet purely mechanical models that he studied in order to gain insights into how walking on two legs works. McGeer described his models as *passive dynamic* meaning that they had neither actuation nor control to represent muscles and the central nervous system; their only source of power was due to the pull of gravity down a gentle slope. One of McGeer's central questions was whether such systems could mimic stable and periodic human gait.

The rimless wheel captures some of the essential mechanical features of human walking; it mimics the foot collisions, falling-and-catching, and inverted pendulum behavior of walking. It does not incorporate, however, leg oscillations or fore-aft instability; *i.e.*, it can stand still on two spokes. The 2D rimless wheel also does not have the lateral instability issues of 3D walking. Despite its simplicity and coarse resemblance to legged locomotion, the 2D rimless wheel is a good first step in a progression to walking models with swinging appendages, various joints, feet, and a torso. It is amenable to simple analyses yielding tidy results in explicit form about periodic motion and stability of a particular system without active energy input or control. The wheel, statically unstable when balancing on one spoke, is stabilized dynamically in the direction of motion by repeated dissipative collisions.

Using linearized equations of motion, accurate when the number of spokes is large and the slope is small ($n \to \infty$ and $\alpha \ll 1$), McGeer found stable limit cycles for downhill rolling at large enough slopes angles. We have extended McGeer's work to a full nonlinear analysis of the wheel for uphill as well as downhill rolling. This analysis adds a slight depth to the discussions of McGeer[6, 7, 8].

The rimless wheel is an example of a mechanical system with intermittent contacts. The spoke impacts give rise to discontinuities in the velocities. The system is piecewise holonomic and conservative, or piecewise-Hamiltonian. Like a 2D disk rolling without slip, in its overall motion, it is holonomic. Globally, it is non-conservative due to the instantaneous loss in energy at each inelastic spoke collision.

Though the 2D rimless wheel is nonlinear in between collisions, it is simply an inverted rigid body pendulum for which a first integral exists - conservation of energy. Thus, one can easily generate the trajectories in between collisions and then piece them together using angular momentum conservation at the collisions to obtain a complete phase space portrait.

From this formulation, we obtain an explicit one-dimensional piecewise continuous Poincaré map that takes a measure of the angular velocity just after a spoke collision to just after the next. The Poincaré map samples the phase space at an angle of rotation fixed by the number of spokes, just after each spoke collision with the ground.

From this map, we obtain results regarding the existence and stability of two possible fixed points corresponding to (1) static equilibrium (at rest on two spokes) and (2) limit cycle (or periodic) motion of the wheel. The existence of these points depends on the model parameters. The birth and death of the fixed points cannot be classified according to classical theory of bifurcation of smooth scalar maps due to discontinuities that can exist in the Poincaré map.

We also find the non-dimensional energy loss per wheel revolution, steady-state non-dimensional speed, and rate of change of speed of the center of mass. We show that in the limit as the number of spokes goes to infinity the rimless wheel behaves like a rolling disk.

The dynamical behavior of the 2D rimless wheel is analogous to that of the classical driven pendulum with damping proportional to speed and constant applied torque [1]. Depending on parameters, both these systems can possess distinct, coexisting, asymptotically stable states whose basins of attraction are separated by the (generalized) stable manifolds of unstable saddle-type solutions. While most of the solutions for the motions and stability of the damped driven pendulum can only be found numerically, nearly all of the solutions explaining the dynamics of the wheel can be found in explicitly soluble form.

This work is a prequel to the study by Coleman *et al.* [2] of the dynamics and stability of a rimless wheel free to move in three dimensions. The 2D limit cycle is also a fixed point of the 3D system. Coleman *et al.* [2] showed that the planar limit cycle of the rimless wheel can also have lateral stability.

2 Description of the System

A planar wheel of axisymmetrically distributed mass m and polar moment of inertia about the center of mass I_C with the rim removed and n evenly spaced spokes of length ℓ, acting as 'legs', rolls in a vertical plane down a slope of angle α under the action of gravity. (See Figure 1.) By *rolling*, we mean motions in which the wheel pivots on one 'support' spoke until another spoke collides with the ground, followed by transfer of support to that spoke, and so on.

Unlike a wheel with a rim, this device cannot roll steadily on a level surface since it loses energy at collisions. We assume the spoke collisions are perfectly inelastic and impulsive, an idealization of foot collisions. Kinetic energy is, thus, lost in each dissipative impact and the wheel's speed is consequently reduced. For completeness, we also allow the wheel to roll backward and forward.

Once a spoke contacts the ground, it maintains hinged contact with the ground until the next spoke collides. When a new spoke collides, we assume that, at that instant, the currently contacting spoke leaves the ground without any impulse. In the model here, we explicitly exclude loss of ground contact and do not allow any slip – unrealistic assumptions for some of the motions. (Allowing for slip and/or loss of contact would limit the maximum slope for no-bounce, no-slip limit cycles to exist. Other, more complicated limit cycles could exist, however.)

2.1 Configuration

The orientation of the wheel is characterized by θ_k, the angle of spoke k measured from the vertical, positive in the counter clockwise sense. θ_k is zero when spoke k is vertical and in contact with the ground. Since the spoked wheel has n-fold symmetry, the angle with the vertical of the spoke presently on the ground in some sense characterizes the configuration of the system.

Special times of interest are just before and just after collision i. $(-)$ and $(+)$ are used as the superscripts to denote these times. For instance, ${}^{i}\theta_k^+$ is the angle of any spoke k, just after collision i. $j(i)$ is the spoke touching the ground just after collision i. For downhill rolling, $j(i) = i$ and $j(i+1) = j(i) + 1$. For uphill rolling, $j(i+1) = j(i) - 1$. ${}^{i}\theta_{j(i)}^+$ is the angle of spoke $j(i)$, the spoke which just collided with the ground at collision i, just after collision i. The overall motion of the wheel is recorded by, say, $\theta_1(t)$.

2.2 Cycle of Motion

A schematic of one cycle, for downhill rolling, is shown in Figure 2. The wheel rotates over the

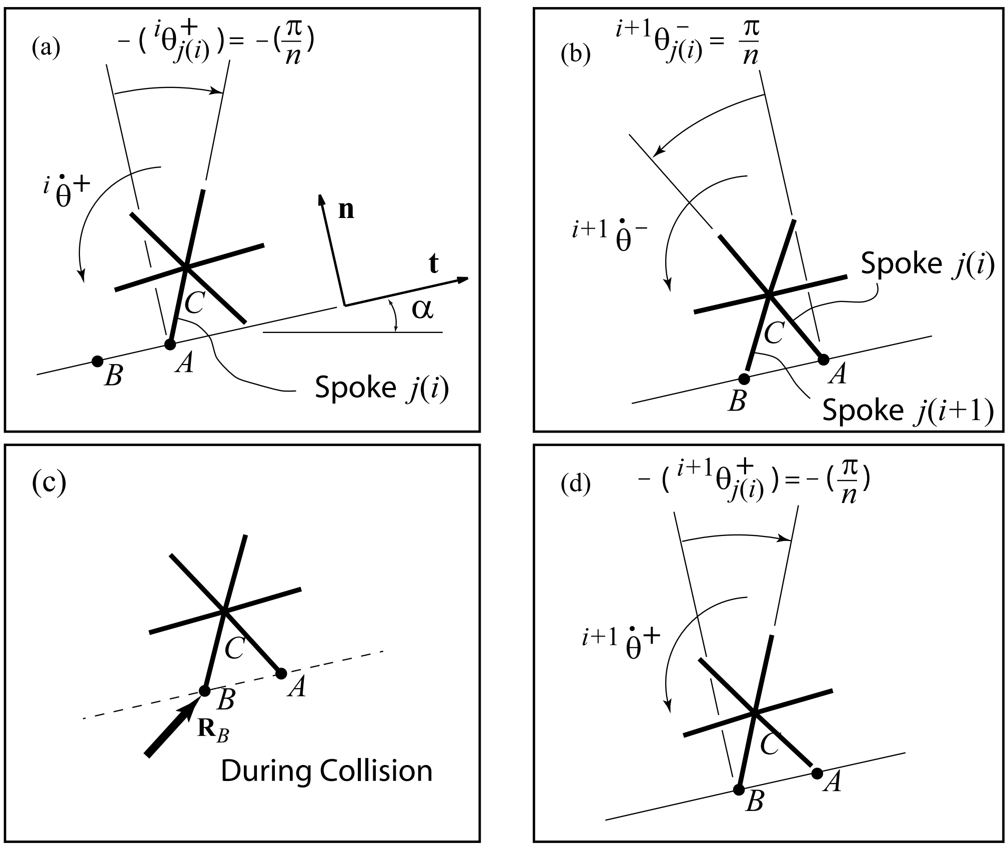

Figure 2: Schematic showing: (a) the state of the wheel over one stride just after the collision of spoke $j(i)$ with point A, (b) the state of the wheel just before collision $i+1$ of spoke $j(i+1)$ at point B, (c) the free body diagram of the wheel during the collision of spoke $j(i+1)$ at point B, and (d) the state of the wheel just after the collision of spoke $j(i+1)$ at point B. The unit vector $\mathbf{n}$ is normal to the slope and the unit vector $\mathbf{t}$ is parallel to the slope.

'stance' spoke, spoke $j(i)$, as an inverted pendulum with initial angle ${}^{i}\theta_{j(i)}^+ = -\pi/n$ and rotation rate $\dot{\theta} = {}^{i}\dot{\theta}_{j(i)}^+$. The non-collisional portion of the stride ends just before the next spoke in sequence, spoke $j(i+1)$, analogous to the swing leg in walking, strikes the ground at ${}^{i+1}\theta_{j(i)}^- = \pi/n$ and $\dot{\theta} = {}^{i+1}\dot{\theta}_{j(i)}^-$ instantaneously transferring support from the trailing spoke to the leading spoke. After impact, the wheel is now poised for the next start-of-cycle at ${}^{i+1}\theta_{j(i+1)}^+ = {}^{i}\theta_{j(i)}^+ = -\pi/n$ and $\dot{\theta} = {}^{i+1}\dot{\theta}_{j(i+1)}^+$. Since the angular velocity of all of the spokes is the same, we will drop subscripts on $\dot{\theta}$ henceforth.

2.3 Motions and Limiting States of the Wheel

When the wheel is rolling *up* or *down*, it may or may not have sufficient energy to pass over the vertical position. When the wheel does not have enough energy to pass the vertical in the downhill direction, the wheel has one motion: reversing direction and then *rocking* back and forth between two spokes. When the wheel does not have enough energy to pass the vertical in the uphill direction, the wheel can have two motions: reversing direction and rocking back and forth between two spokes, as above, or reversing direction and rolling downhill.

If the wheel completes a downhill cycle, the kinetic energy(KE) of the wheel just before collision is greater than the kinetic energy at the start-of-cycle due to the downhill slope ($KE^-_{i+1} > KE^+_i$). The kinetic energy of the wheel drops instantaneously at impact, however. For downhill motions, the following outcomes are possible.

1. Periodic motion arises if the energy lost in collision is exactly balanced by the kinetic energy gained in falling. In this case, the state variables are equal to those at the start of the previous stride. The wheel is in periodic or limit cycle motion that repeats indefinitely.

2. If more energy is lost in collision than gained in falling, the wheel slows, either toward a periodic motion or to an eventual stop on two spokes, depending on the slope, inertia, and number of spokes.

3. If more energy is gained in falling than lost in collision, we expect the wheel to increase in speed toward the periodic motion.

4. For a particular angular velocity after collision and small enough slope, the wheel will approach the unstable vertical equilibrium in infinite time.

For uphill motions, the wheel will eventually reverse direction, roll downhill, and reach one of the outcomes above for downhill rolling.

Thus, the possible limiting states for the wheel are limit cycle motion, the stopped position on two spokes, and the unstable vertical equilibrium. Limit cycles and the stopped position correspond to the condition ${}^{i+1}\dot{\theta}^+ = {}^{i}\dot{\theta}^+$ and ${}^{i+1}\theta^+ = {}^{i}\theta^+ = -\frac{\pi}{n}$; *i.e.*, the state of the wheel is the same just after every collision i.

2.4 Behaviors of the Wheel

The behaviors of the wheel are the ways in which the wheel approaches the possible limiting states. They depend upon the wheel parameters *and* initial conditions. For example, the wheel can roll down the slope at higher than the angular rate needed to just reach the vertical position in infinite time but less than the limit cycle angular rate, increase in speed and approach a limit cycle from below. Using our notation, we can represent the behavior schematically as Down$\xrightarrow{+}$ Limit Cycle where the (+) or (−) refers to increasing or decreasing angular velocity after each collision. Using our shorthand notation, we summarize the behaviors of the wheel in Figure 3(a) and illustrate them schematically in Figure 3(b).

In cases 3, 4, and 5, the wheel rocks back and forth on two spokes until coming to rest on two spokes after an *infinite* number of collisions in *finite* time. Since, as we will see, support transfer produces a simple ratio (less than one) between adjacent terms in the sequence of angular rates, the rocking cannot stop in a finite number of collisions. But, it can stop in finite time since the total time of rocking is an infinite geometric series that has a finite sum. McGeer [9] finds the finite sum of this infinite series, obtained from a linearized analysis of rocking, with arbitrary accuracy for the case where the angular rate has gotten very small after some large but finite number of collisions.

Cases 10 and 11 can only happen with three and four spoked wheels and sufficiently small radius of gyration. In these special cases, the wheel comes to a stop after the first spoke collision, for any initial conditions.

(a)

1. Down $\xrightarrow{+}$ Limit Cycle
2. Down $\xrightarrow{-}$ Limit Cycle
3. Down $\longrightarrow$ Rock $\longrightarrow$ Stop
4. Rock $\longrightarrow$ Stop
5. Up $\longrightarrow$ Rock $\longrightarrow$ Stop
6. Up $\longrightarrow$ Down $\xrightarrow{+}$ Limit Cycle
7. Down $\longrightarrow$ Vertical
8. Up $\longrightarrow$ Vertical
9. Up $\longrightarrow$ Down $\longrightarrow$ Vertical
10. Up $\longrightarrow$ Stop
11. Down $\longrightarrow$ Stop

(b)

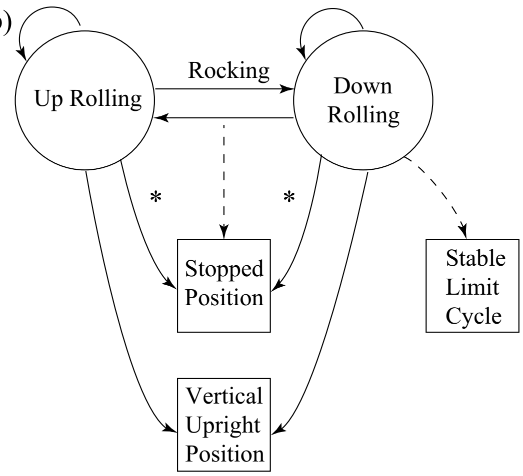

Figure 3: (a) The 11 possible wheel behaviors. (b) Diagram showing the possible motions, the condition of rocking, and the possible limiting states: stopped on two spokes, the limit cycle, and the vertical position. Solid arrows indicate that a motion or limiting state can be reached in finite time after one collision or in infinite time before the next collision can occur. Dotted arrows indicate that a limiting state is reached asymptotically after infinite collisions in finite time. The asterisks next to a solid arrow indicate that the stopped position can be reached in one collision;*e.g.*, cases 10 and 11 in (a). The arrows turning back on themselves and attached to the motions indicate that the motion can occur over one or more iterations.

3 Governing Equations and the Phase Space

Since the rimless wheel has n-fold symmetry, the wheel looks the same for a given angle of any spoke that is currently in contact with the ground between collisions. The angle with the normal to the slope of the spoke presently on the ground in between collisions, then, can be used to characterize the configuration of the system, as noted in Section 2.1. As the center of rotation of the rimless wheel is instantaneously moved with each collision from the tip of one spoke to the next, we thus consider the orientation of the wheel between collisions restricted to the interval $I = [-\pi/n, \pi/n]$ over many collisions by resetting the angle at each collision. The boundaries of the interval are determined by n, the number of spokes.

3.1 Equation of Motion between Collisions

Referring to Figure 2, we derive the non-dimensional equation of motion from angular momentum balance about point A:

$$\ddot{\theta} - \sin(\theta + \alpha) = 0, \qquad |\theta| < \pi/n. \tag{1}$$

where

$$3 \leq n < \infty, \text{ and } 0 \leq \alpha \leq \pi/2. \tag{2}$$

An overdot indicates differentiation with respect to non-dimensional time $\tau = t\sqrt{mg\ell/(I_C + m\ell^2)}$. This equation is simply that of an inverted rigid body pendulum.

3.2 Collision Transition Conditions

The angle is reset at each collision $i+1$ as support is transferred from spoke $j(i)$ to $j(i+1)$ according to the following mapping:

$$\theta \mapsto -\theta, \qquad |\theta| = \pi/n. \tag{3}$$

We obtain this relation by noting that the orientation of the wheel is rotated by $-\frac{2\pi}{n}$ after a downhill collision and by $\frac{2\pi}{n}$ after an uphill collision.

Ignoring the impulse due to gravity during collision, we derive the condition relating the angular velocity of the wheel before and after collision from the conservation of angular momentum during collision about the incipient point of spoke contact, point B in Figure 2:

$$\dot{\theta} \mapsto \mu\dot{\theta}, \qquad |\theta| = \pi/n \tag{4}$$

where

$$\mu = \frac{I_C + m\ell^2\cos(\frac{2\pi}{n})}{I_C + m\ell^2} = 1 + \lambda^2\left(\cos\left(\frac{2\pi}{n}\right) - 1\right), \qquad 0 \leq \mu < 1. \tag{5}$$

and $\lambda^2 = \frac{1}{\frac{I_C}{m\ell^2}+1}$. Henceforward, we will call λ^2 the *moment of inertia parameter.*

To consider reasonable moment of inertia values, we could assume that $0 \leq \frac{I_C}{m\ell^2} \leq 1$[1]. For this range of values, $\frac{1}{2} \leq \lambda^2 \leq 1$. For each number of spokes, there is a minimum value of μ that exists for $\lambda^2 = 1$ (since $\lambda^2 > 0$ and $\cos(\frac{2\pi}{n}) < 1$): $\mu_{\min} = \cos(\frac{2\pi}{n})$. Figure 9(b) shows these minimum values of μ.

The non-dimensional collision parameter μ in Equation (4) represents energy lost during impact since it is always less than one, except when the number of spokes is infinity so that μ is equal to one. We discuss physical behaviors of the rimless wheel for special values of μ in Section 6.3; in particular, we consider $n = 3$ and $\frac{2}{3} < \lambda^2 \leq 1$ which give the unusual case $-0.5 \leq \mu < 0$.

3.3 The Phase Space and Trajectories

The classical rigid body pendulum has the usual phase space with coordinates $(\theta, \dot{\theta})$, as does the rimless wheel if we keep track of its overall angle. To have the points of the phase surface correspond directly to states of the physical system, it is better to represent the state of a pendulum on a phase cylinder since for every rotation by 2π, the pendulum has the same physical orientation. Similarly, since a rotation of the wheel about the contact point of the spoke currently touching the ground by $2\pi/n$ leaves the wheel in the same physical orientation just displaced down or up the slope, we can reset the configuration angle of the rimless wheel at each collision to correspond to the physical state.

We make the following change of variables for the wheel, however, that simplifies the definition and interpretation of the Poincaré map we construct subsequently:

$$z(\dot{\theta}) = \dot{\theta}^2\mathrm{sgn}(\dot{\theta}). \tag{6}$$

We will refer to z (taken to be the square of the angular rate times its sign) as the *measure of angular velocity*, henceforward. The absolute value of the measure of angular velocity ($|z|$) is simply twice the non-dimensional total kinetic energy of the wheel.

Thus, the evolution of the trajectories for the rimless wheel can be studied on U, a subset of phase space that can also be bent around into a cylinder, just smaller in diameter than that of the pendulum:

$$U = \{(\theta, z)| \quad |\theta| \leq \pi/n\}. \tag{7}$$

(If we rescale the angle by the number of spokes, say $\Theta = n\theta$, then the cylinder is of the same diameter as for the pendulum.) The boundaries of U are $\partial U = \{(\theta, z)| \quad |\theta| = \pi/n\}$.

Rewriting Equation (1) in first order form and combining it with the collision transition functions Equations (3) and (4), the (θ, z) phase flow is governed by

$$\begin{aligned} \dot{\theta} &= \mathrm{sgn(z)}\sqrt{|\mathrm{z}|}, & |\theta| < \pi/\mathrm{n} \qquad (8)\\ \dot{z} &= 2\sqrt{|z|}\sin(\theta + \alpha) & \\ (\theta, z) &\mapsto (-\theta, \mu^2 z), & |\theta| = \pi/n \qquad (9) \end{aligned}$$

[1]In practice, however, one could construct a special rimless wheel with $\frac{I_C}{m\ell^2} > 1$ as follows. Join, rigidly, two identical rimless wheels (in parallel planes with spokes aligned and sharing a common central axis) to a third body (also with an axisymmetric mass distribution but diameter larger than the spoke length ℓ) located symmetrically between them. Then put two identical ramps side by side allowing the central body to pass freely down between the ramps while the two rimless wheels make contact with the ramps.

We can re-write Equation (8) as

$$\dot{\mathbf{q}} = \mathbf{g}(\mathbf{q}) \tag{10}$$

where $\mathbf{q} = \{\theta, z\}^T$ is the state vector and $\mathbf{g} : U \to U$ is a time-independent vector field. We further define the transition function as the map $\mathbf{h} : \partial U \to \partial U$ where $\mathbf{h}$ is prescribed by Equation (9). [Note: there is the small caveat with this change of variables that, for $\alpha > \frac{\pi}{n}$ where the wheel can roll downhill from the rest position on two spokes with no initial speed, the first order system Equation (8) cannot be integrated forward numerically since $z_0 = 0$. Generating phase space portraits with this formulation is not troublesome, nevertheless, since in practice one can set $z = \epsilon$ where ϵ is a very small positive number; or, the trajectories can be generated as below.]

The evolution of the system is a sequence of trajectory segments where the endpoint of one segment is connected to the initial point of the next by the instantaneous application of the collision rule. The flow in phase space between collisions is easily generated using the first integral of motion(conservation of energy) obtained from Equation (10):

$$|z| = |z_0| + 2(\cos(\theta_0 + \alpha) - \cos(\theta + \alpha)). \tag{11}$$

All trajectories start in U and terminate in U.

Figure 4 shows representative phase space portrait for several initial conditions; the phase cylinder is unfurled to more easily visualize it. The phase space portraits have the following features:

- The nature of the phase space portrait and, hence, the physical behavior of the wheel depend only on the slope angle α, the number of spokes n, and the damping parameter μ.
- Every trajectory segment terminates on ∂U except for those on the separatrix segments which initiate on ∂U at

  $$^{dn}z = 2(1 - \cos(\alpha - \frac{\pi}{n})), \quad \theta = -\pi/n \tag{12}$$

  or

  $$^{up}z = -2(1 - \cos(\alpha + \frac{\pi}{n})), \quad \theta = \pi/n. \tag{13}$$

  and terminate at the unstable equilibrium $(\theta, z) = (-\alpha, 0)$. If $\alpha > \frac{\pi}{n}$, the unstable equilibrium is not in U.

  ^{dn}z is the downhill measure of angular velocity just after collision, and ^{up}z the uphill measure of angular velocity just after collision, such that the wheel reaches the vertical position in infinite time. We obtain these critical values using conservation of energy; all of the kinetic energy of the wheel following a spoke collision is converted to potential energy at $\theta = -\alpha$.
- The sequence of trajectory and separatrix segments on the phase cylinder do not form continuous continuous curves on the phase cylinder due to the instantaneous drop in energy at each collision.

In Figure 5, θ and z are plotted versus non-dimensional time τ corresponding to trajectory $\gamma_1(t)$ in Figure 4.

4 Poincaré Section and Return Map

For a constant torque, damped pendulum, finding limit cycles that encirclethe cylinder and determining their number and stability can be accomplished by constructing a return map (or iterative function) along a vertical slice at a given angle, or Poincaré section, of the phase cylinder (see Andronov, *et al.* [1]); McGeer applied the same approach to the linearized equations for the wheel for downhill rolling. To study the full nonlinear system for both uphill and downhill rolling, we also use the method of a Poincaré section Σ. The one degree of freedom rimless wheel has a phase cylinder with coordinates $(\theta, z) \in U$. Instead of taking a Poincaré section at fixed intervals of time, a natural place to sample this surface is at the points of discontinuity, the collisions, where we know the orientation of the wheel: $\theta = -\frac{\pi}{n}$ after a downhill collision and $\theta = \frac{\pi}{n}$ after an uphill one.

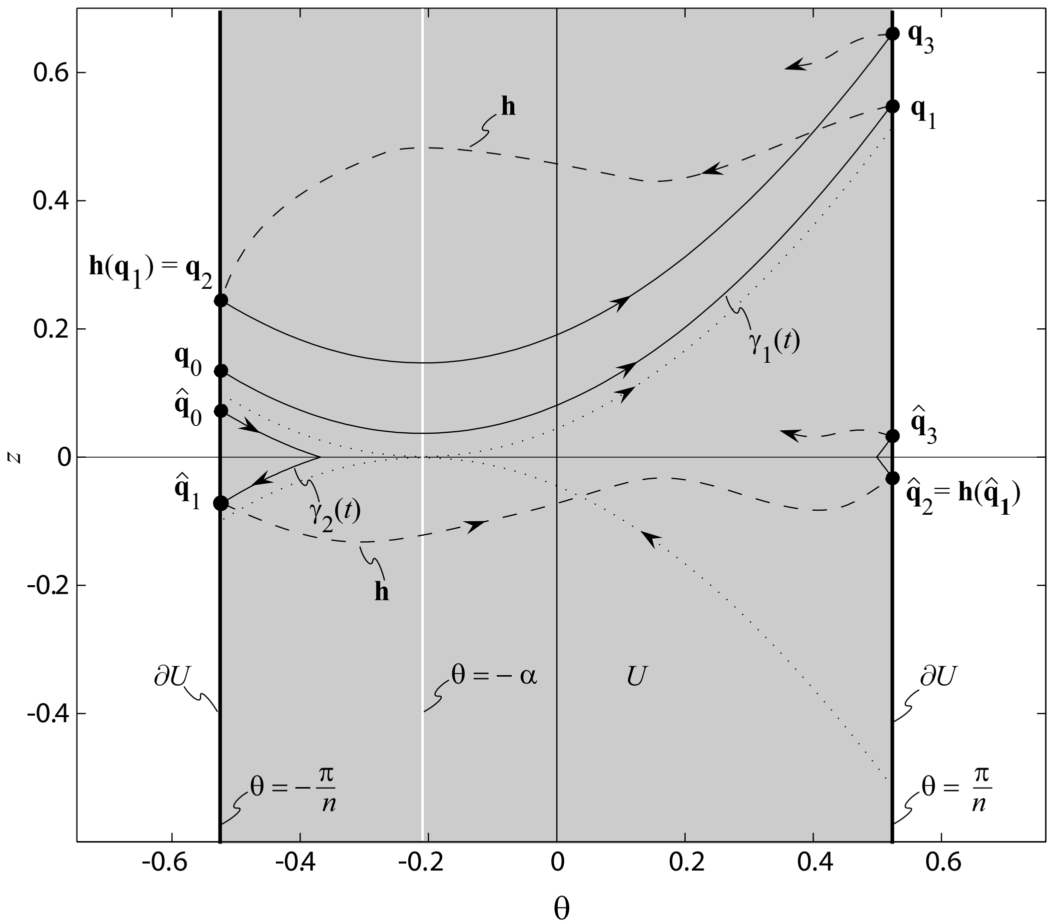

Figure 4: Two phase space trajectories in U. The trajectories are labeled $\gamma_1(t)$ and $\gamma_2(t)$ and both have $\mu = \frac{2}{3}$, $n = 6$, and $\alpha = \frac{\pi}{15}$. The initial condition for the first trajectory is $\gamma_1(t_0) = \mathbf{q}_0 = (-0.5236, 0.135)$ and subsequent points of the trajectory on the boundary of U are denoted by $\mathbf{q}_i$, $i = 1, 2, 3, \ldots$. The initial condition for the second trajectory is $\gamma_2(t_0) = \hat{\mathbf{q}}_0 = (-0.5236, 0.0726)$ and subsequent points of the trajectory on the boundary of U are $\hat{\mathbf{q}}_i$, $i = 1, 2, 3, \ldots$. The *solid* lines are integral curves of the vector field $\mathbf{g}$ representing the motion between collisions and the *dashed* lines are fictitious 'curves' that piece together the integral curves at collisions to make a complete trajectory. The dashed lines represent the instantaneous application of the transition function $\mathbf{h}$ at each collision that manifests itself as a decrease in angular velocity. The *dotted* lines are trajectories that correspond to the separatrices for a rigid body pendulum with ${}^{dn}z = 0.09789$ and ${}^{up}z = -0.51371$. If the wheel starts at initial conditions that are on these trajectories, the wheel either reaches the vertical unstable equilibrium $\theta = -\alpha$ in infinite time or leaves the vertical position and makes a collision in finite time. The arrows on the trajectories indicate the forward direction in time. The solid white line indicates the vertical position of the wheel.

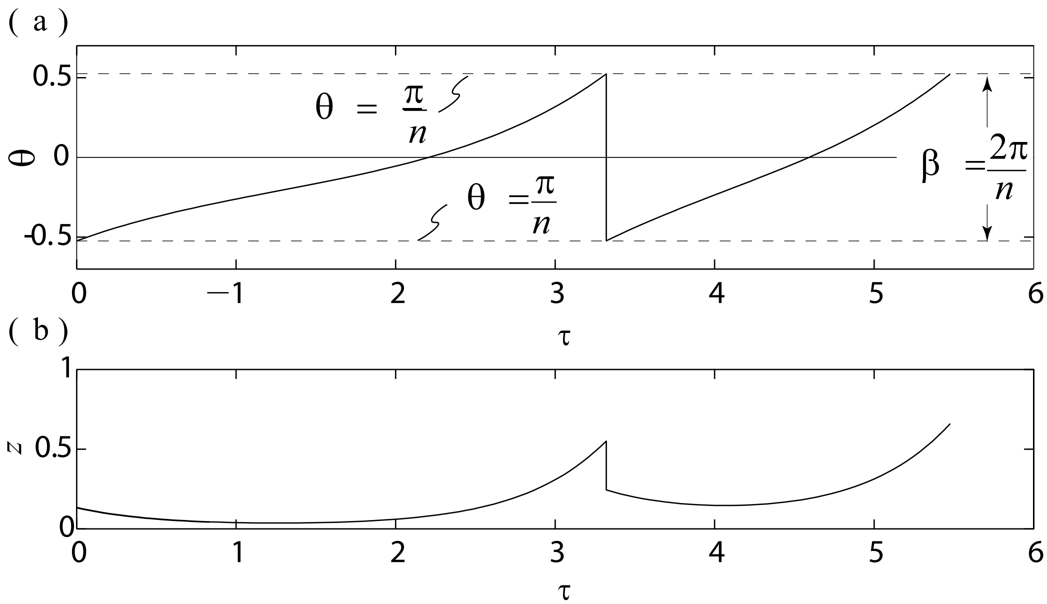

Figure 5: In figures (a) and (b), θ and $\dot{\theta}$ are plotted, respectively, versus non-dimensional time, τ, corresponding to trajectory $\gamma_1(t)$ in Figure 4. In the time interval shown, the wheel makes two collisions. The plots show the discontinuities in the state variables at the collisions. The first plot shows that θ is bounded by $\theta = -\frac{\pi}{n}$ and $\theta = \frac{\pi}{n}$ and that the angle is reset after each collision according to Equation (3), the collision transition rule. The size of the interval is equal to the angle between the spokes, $\beta = \frac{2\pi}{n}$.

4.1 The Poincaré Section

We thus define the sampling location in the phase space, the Poincaré section Σ, as:

$$\Sigma = \left\{ (\theta, z) \,\middle|\, \begin{array}{c} \theta = -\frac{\pi}{n}, \quad z \geq 0, \quad \text{and} \quad z \neq {}^{dn}z \\ \theta = \frac{\pi}{n}, \quad z < 0, \quad \text{and} \quad z \neq {}^{up}z \end{array} \right\}. \tag{14}$$

The critical values of angular velocity after collision, ${}^{dn}z$ and ${}^{up}z$, defined above, are excluded from the Poincaré section because once the wheel attains either of the critical values after a collision, the wheel will not have any more collisions since the wheel reaches the vertical in infinite time. Thus, we cannot sample the space after collisions since the wheel has stopped in the vertical position.

The flow of the differential equation is everywhere transverse to Σ; *i.e.* the phase space trajectories pass through the Poincaré section. This is easily seen by considering the vector field in (θ, z) space on Σ given by Equation (8). The flow is transverse to Σ since $\left.\frac{dz}{d\theta}\right|_{\theta=\pm\frac{\pi}{n}}$ is defined.

4.2 The Poincaré Map

Orbits in the phase space will be studied by considering the mapping

$$\mathbf{f} : \Sigma \to \Sigma \tag{15}$$

induced by the solutions of Equation (1). The Poincaré map takes the form:

$${}^{i+1}\mathbf{q}^{+} = \mathbf{f}({}^{i}\mathbf{q}^{+}) \quad \text{or} \quad {}^{i}\mathbf{q}^{+} \overbrace{\xrightarrow{\mathbf{p}} {}^{i+1}\mathbf{q}^{-} \xrightarrow{\mathbf{h}}}^{\mathbf{f}} {}^{i+1}\mathbf{q}^{+}. \tag{16}$$

where $\mathbf{q} = \{{}^{i}\theta^{+}_{j(i)}, {}^{i}z^{+}\}^{T} \in \Sigma$. $\mathbf{f}$ is a composition of two maps: $\mathbf{f} = \mathbf{h} \circ \mathbf{p}$, where $\mathbf{p}$, obtained by integrating the equations of motion, describes the motion following collision i to just before collision $i+1$, and $\mathbf{h}$ governs the jump in the state vector incurred at collision $i+1$.

Figure 6 shows the phase space and the section Σ. Positive orbits are sequences of the angular velocity of wheel after each collision. The sequences are obtained by iterating forward from an initial condition in Σ using the Poincaré map $\mathbf{f}$. The orbits can be visualized by marking the sequences of the measures of angular velocity on the Poincaré section. Consider orbits with initial measures of angular velocity just after collision ${}^0z^+ \in \Sigma$ in Figure 6: Positive orbits from initial conditions with ${}^0z^+ > {}^{dn}z > 0$ and ${}^{up}z <^0 z^+ < {}^{dn}z$ are shown for several iterates with $\alpha \leq \frac{\pi}{n}$.

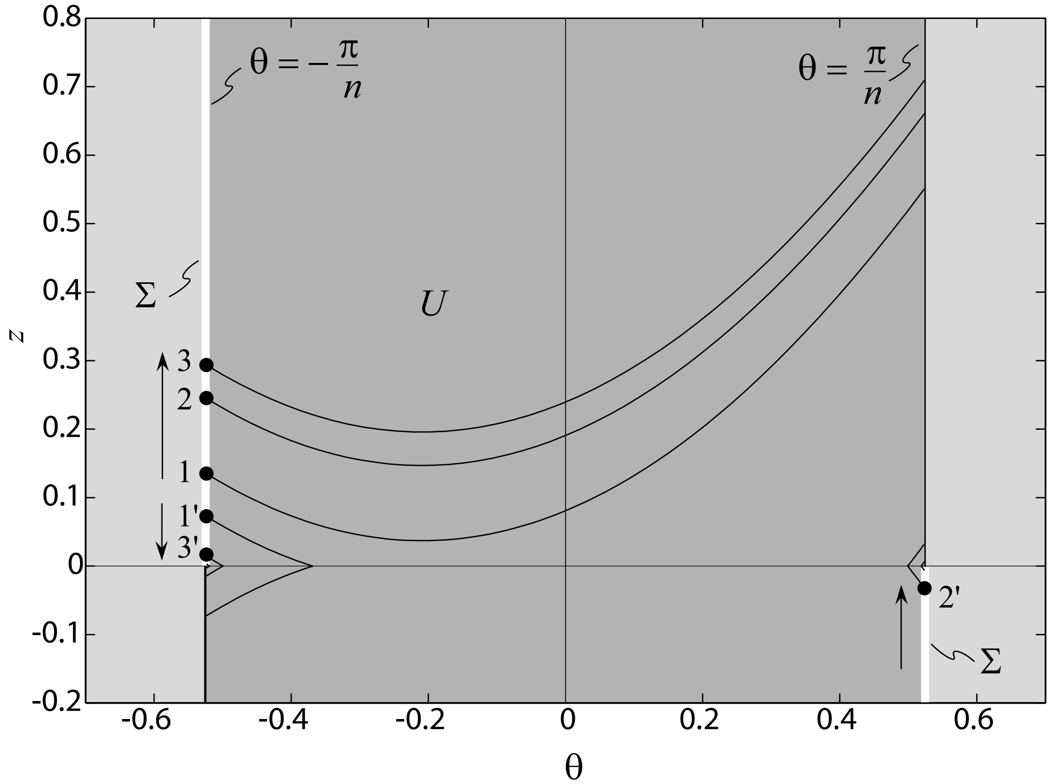

Figure 6: The phase space $(\theta, z) \in U$ showing the Poincaré section Σ. The solid white vertical lines indicate Σ. Positive orbits from initial conditions ${}^0z^+ > {}^{dn}z > 0$ and ${}^{up}z < {}^0z^+ < {}^{dn}z$ are shown for several iterates with $\alpha = \frac{\pi}{15}$, $\mu = \frac{2}{3}$, and $n = 6$. In this case, ${}^{dn}z = 0.255$ and ${}^{up}z = -0.585$. The orbits in Σ starting with with ${}^0z^+ = 0.09$ and $z_i = 0.0484$ are marked by the sequences, $1, 2, 3, \ldots$ and $1', 2', 3', \ldots$, respectively. The orbit starting with ${}^0z^+ = 0.09 > {}^{dn}z$ corresponds to the wheel starting off downhill and approaching a limit cycle. The orbit starting at ${}^0z^+ = 0.0484 < {}^{dn}z$ corresponds to starting off downhill with too little energy to make it past the vertical position and rocking back and forth between two spokes, eventually coming to rest.

The map $\mathbf{f}$ can be reduced from a two-dimensional to one-dimensional map since the section is taken at a known angle $({}^i\theta^+_{j(i)} = \pm\frac{\pi}{n}))$. We define the scalar map as $P : \Sigma \to \Sigma$, which updates the measure of the angular velocity at each collision. The section we have defined is used since the first integral of motion, the conservation of energy, exists for motion between collisions and since the transition function for the angular velocity at each collision is simple. Thus, the map can be obtained easily in closed form.

4.2.1 Constructing the Return Map P

We are looking for the map P in a form given schematically as the difference equation

$$ {}^{i+1}z^+ = P({}^iz^+), \quad {}^iz^+ \in \Sigma. \tag{17} $$

To further ease notation, we let $Z = {}^i z^+$. We will refer to Z as the *measure of angular velocity just after collision*, henceforward.

The map P can be piecewise continuous depending upon the slope angle: due to the change in variables of Equation (6), P is at least piecewise linear in Z (rather than piecewise quadratic in $\dot{\theta}$). The map P depends on slope angle and measure of angular velocity as follows:

1. $\alpha \leq \frac{\pi}{n}$: P is piecewise linear over three intervals of Z.
   (a) $Z > {}^{dn}Z$ or $Z < {}^{up}Z$: the wheel has enough energy after a collision to make it past the vertical in the downhill or uphill direction, respectively. To construct this piece of the map, conservation of energy takes the measure of angular velocity of the wheel just after collision i to just before collision $i+1$ and, then, the collision transition condition, $z \rightarrow \mu^2 z$, takes the measure of angular velocity just before collision $i+1$ to just after collision $i+1$. This part of the map will reflect the wheel's downhill gain or uphill loss in kinetic energy between collisions and the instantaneous loss in kinetic energy due to collisions.
   (b) ${}^{up}Z < Z < {}^{dn}Z$: the wheel does not have enough energy after a collision to make it past the vertical in the uphill or downhill direction, and consequently reverses direction in between collisions. To construct this part of the map, conservation of energy between collisions gives us that the measure of angular velocity just after collision i is equal in magnitude but opposite in sign to the measure of angular velocity just before collision $i+1$ and, again, the collision transition condition, $z \rightarrow \mu^2 z$, takes the angular velocity just before collision $i+1$ to just after collision $i+1$.
2. $\alpha > \frac{\pi}{n}$: P is linear for all Z. The slope is so large that the center of mass is always past the vertical for downhill rolling and never makes it past the vertical for uphill rolling.
   (a) $Z \geq 0$: the wheel always gains kinetic energy between collisions and never reverses direction when starting downhill.
   (b) $Z < 0$: the wheel always loses kinetic energy between uphill collisions. If it does not have enough energy to make it to the next uphill collision, it makes one reversal and rolls down hill as above: the reversal occurs for $-4\sin\alpha\sin\frac{\pi}{n} < Z < 0$.

In functional form, we thus summarize the map P as:

$$P(Z) = \begin{cases} \mu^2(Z + 4\sin\alpha\sin\frac{\pi}{n}) & \alpha \leq \frac{\pi}{n} \text{ and } Z > {}^{dn}Z > 0 \text{ or } Z < {}^{up}Z < 0, \text{ or} \\ & -\infty < Z < \infty \text{ and } \alpha > \frac{\pi}{n}. \\ -\mu^2 Z & \alpha \leq \frac{\pi}{n} \text{ and } {}^{up}Z < Z < {}^{dn}Z. \end{cases} \tag{18}$$

The piecewise linearity of the map makes its graphical construction and interpretation easier. We show the details of the Poincaré map for one parameter set in Figure 7. Three intervals of the measure of angular velocity, Z, are shown on the graph:

1. In the first interval, $Z < {}^{up}Z$, the wheel has enough energy to make it past the vertical in the uphill direction and $P(Z) = \mu^2(Z + 4\sin\alpha\sin\frac{\pi}{n})$.
2. In the second interval, ${}^{up}Z < Z < {}^{dn}Z$, the wheel does not have enough energy to make it past the vertical position in the uphill or downhill direction and $P(Z) = -\mu^2 Z$.
3. In the third interval, $Z > {}^{dn}Z$, the wheel has enough energy to make it past the vertical in the downhill direction and $P(Z) = \mu^2(Z + 4\sin\alpha\sin\frac{\pi}{n})$.

The graph shows a stair-step diagram, with initial condition Z_1; the progress of the wheel can be traced by following the dotted line on the diagram:

1. The wheel starts off uphill with initial measure of angular velocity Z_1 in the first interval.
2. The wheel makes it past the vertical and has a collision with the slope and emerges with a new measure of angular velocity $Z_2 = P(Z_1)$ in the second interval.

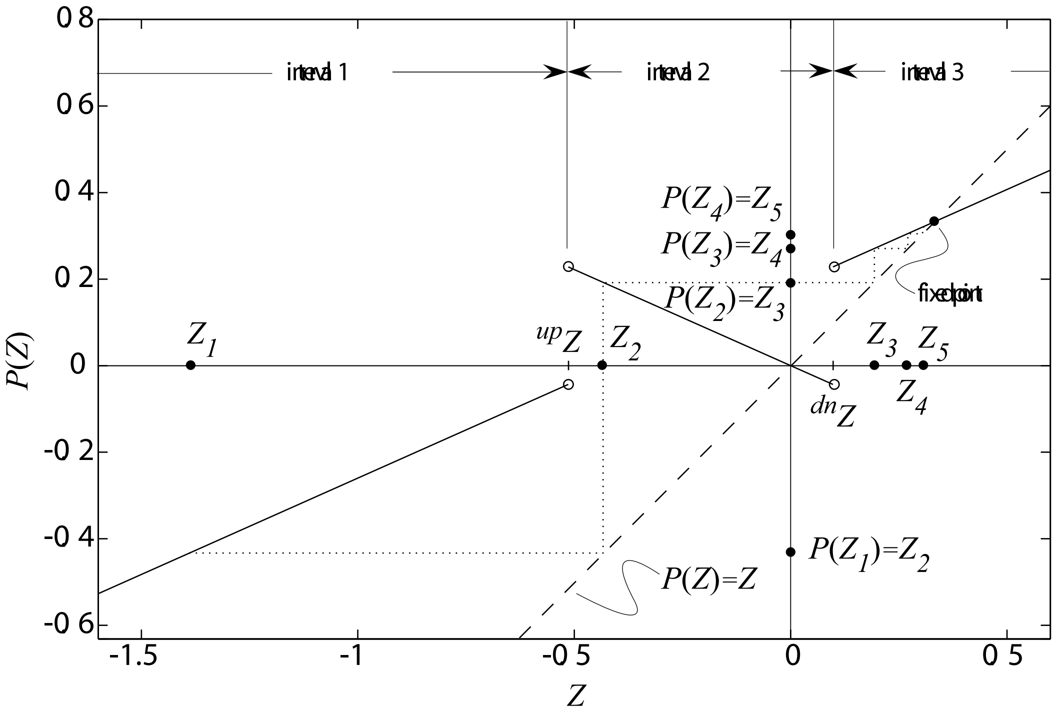

Figure 7: The graph of the Poincarè map with $\mu = \frac{2}{3}$, $n = 6$, and $\alpha = \frac{\pi}{15} < \frac{\pi}{6}$. Three intervals of the measure of velocity after each collision, Z, are shown: (1) $Z < {}^{up}Z < 0$, (2) ${}^{up}Z < Z < {}^{dn}Z$, and (3) $Z > {}^{dn}Z$. A stair-step diagram is shown with initial condition Z_1 for several iterations. The wheel starts off uphill at initial value Z_1, makes it past the vertical, collides with the slope, and emerges with $P(Z_1) = Z_2$. The wheel does not make past the vertical now, reverses direction, collides with the slope, and emerges with $P(Z_2) = Z_3$. Thereafter, it continues to make it past the vertical position after each collision increasing its angular velocity as it goes until it converges to the fixed point shown on the diagram. The fixed point is at the intersection of the graph with the identity line, $P(Z) = Z$.

3. The energy lost to the collision does not leave the wheel with enough energy to make it past the vertical. It reverses direction and makes another collision with the slope leaving the wheel with the next measure of velocity $Z_3 = P(Z_2)$ in the third interval. The wheel now has enough energy to make it past the vertical in the downhill direction.

4. The wheel rolls downhill and makes repeated collisions with the slope and so on until the wheel converges to a steady-state measure of angular velocity after an infinite number of collisions in finite time. The fixed point is marked by the intersection of the graph of P with the identity line $P(Z) = Z$.

In short, the wheel rolls uphill, collides with the slope, reverses direction, rolls downhill and converges to the limit cycle from below. Previously, we denoted this motion in Section 2.4 as Up$\rightarrow$ Down$\xrightarrow{+}$ Limit Cycle.

Refer to Figure 8 to see a comparison of the graph described above to other typical Poincarè map graphs, as well as a few special cases, for a few characteristic slope angles. (We discuss the terminology and important features of this figure subsequently in Section 5 on fixed points of the return map and stability, Section 6 on the existence of fixed points, and Section 6.3 on special parameter cases.)

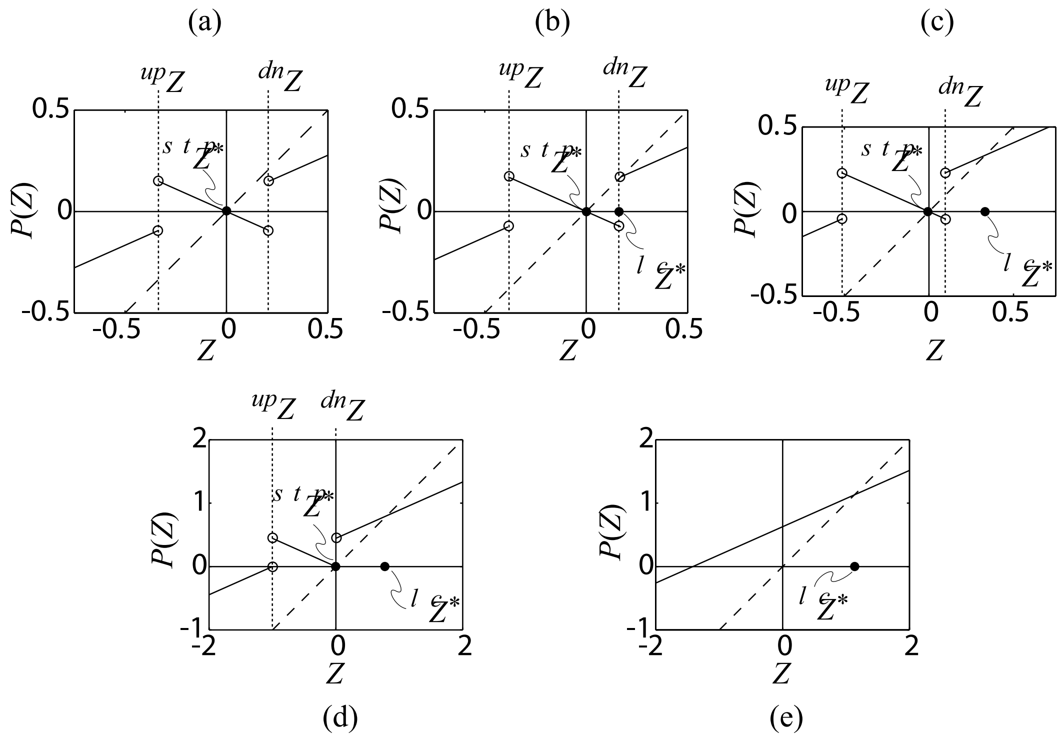

Figure 8: Five typical graphs of the Poincarè map, $P(Z)$ versus Z, with $n = 6$ and $\mu = \frac{2}{3}$. The open circles indicate that the maps are not defined at these locations. **Note: the scales are different in each graph.** (a) Small slope angle $\alpha = \frac{\pi}{50} < \alpha_c$, showing the piecewise linearity, the two discontinuities at $Z = {}^{up}Z$ and $Z = {}^{dn}Z$, and the fixed point ${}^{stp}Z^* = 0$. (b) Small slope angle $\alpha = \alpha_c = 0.1071$, showing again the piecewise linearity, the two discontinuities at $Z = {}^{up}Z$ and $Z = {}^{dn}Z$, and the fixed point ${}^{stp}Z^* = 0$. However, in this case where the slope angle is exactly equal to the critical angle, the map just 'kisses' the identity line at the limit cycle fixed point ${}^{lc}Z^* = {}^{dn}Z$. (c) Intermediate slope angle $\alpha = \frac{\pi}{15}$, showing again the piecewise linearity, the two discontinuities of the map at ${}^{dn}Z = 0$ and ${}^{up}Z$, and both fixed points ${}^{stp}Z^* = {}^{dn}Z = 0$ and ${}^{lc}Z^*$. This is the case discussed in detail in Section 4.2.1 and Figure 7. (d) Intermediate slope angle $\alpha = \frac{\pi}{6} = \frac{\pi}{n}$, showing again the piecewise linearity, the two discontinuities of the map at ${}^{dn}Z = 0$ and ${}^{up}Z = -4\sin^2\frac{\pi}{n} = -1$, and both fixed points ${}^{stp}Z^* = {}^{dn}Z = 0$ and ${}^{lc}Z^*$. The only initial condition that will give ${}^{stp}Z^*$ is $Z = 0$; *i.e.*, starting at rest. (e) Steep slope angle $\alpha = \frac{\pi}{4} > \frac{\pi}{n}$, showing the linearity of the map for all Z and one fixed point ${}^{lc}Z^*$; ${}^{stp}Z^* = 0$ cannot exist for $\alpha > \frac{\pi}{n}$.

5 Fixed Points and Stability

The limiting states, limit cycle motion and the eventual stopping of the wheel, are fixed points of the map P, since, for each of these limiting states, the state of the wheel is the same after every collision. The unstable vertical equilibrium is not a fixed point of P, however, since the wheel does not complete a cycle in that case. (Again, the vertical position is, however, an unstable equilibrium of the system describing the motion *in between* collisions.)

5.1 Fixed Points of P

A point Z^* is a fixed point of P if $P(Z^*) = Z^*$. The possible fixed points of P are:

$$Z^* = \begin{cases} {}^{lc}Z^* \equiv \frac{4\mu^2 \sin\frac{\pi}{n}\sin\alpha}{1-\mu^2} > 0 \\ {}^{stp}Z^* \equiv 0, \end{cases} \quad . \tag{19}$$

The non-zero fixed point ${}^{lc}Z^*$ is the measure of angular velocity after each collision that corresponds to the limit cycle motion. The limit cycle is unique for fixed parameters. The limit cycle is approached monotonically from above or below as the wheel rolls down the slope. The zero fixed point ${}^{stp}Z^*$ is the measure of angular velocity that corresponds to the stopped position of the wheel at rest on two spokes. The stopped position is approached monotonically as the wheel rocks back and forth between two spokes. The angular velocities corresponding to the fixed points are ${}^{lc}\dot{\theta}^* = \sqrt{{}^{lc}Z^*} > 0$ and ${}^{stp}\dot{\theta}^* = {}^{stp}Z^* = 0$.

We specify the ranges of slope angles for which the limit cycle and stopped condition fixed points exist and the initial conditions which are attracted to the fixed points in subsequent sections.

5.2 Stability of the Fixed Points

The stability of a fixed point of a scalar map is determined by the first derivative of the map evaluated at that point. A fixed point Z^* of P is asymptotically stable if the absolute value of the first derivative of the map evaluated at the fixed points is less than one, $|DP(Z^*)| < 1$. The first derivative of the map P at the fixed points ${}^{lc}Z^*$ and ${}^{stp}Z^*$ is

$$DP(Z^*) = \begin{cases} \frac{dP}{dZ}\big|_{Z={}^{lc}Z^*} = \mu^2 \\ \\ \frac{dP}{dZ}\big|_{Z={}^{stp}Z^*} = -\mu^2 \end{cases} . \tag{20}$$

Since the collision parameter μ is always less than one, $0 \leq \mu < 1$, the first derivative of the map at the fixed points is always less than one, $|DP(Z^*)| < 1$. Both fixed points of P, ${}^{lc}Z^*$ and ${}^{stp}Z^*$ are, thus, asymptotically stable.

6 Existence of Fixed Points and Their Basins of Attraction

The explicit construction of the return map enables the definition of: (1) precise conditions on the wheel parameters for the existence of the fixed points (described qualitatively in Section 2.3) and (2) the basins of attraction for the fixed points in the intermediate slope angle regime.

6.1 Slope Angle and Existence of the Fixed Points

So far, (for any $n \geq 3$ and $0 < \mu < 1$), we have the following conditions on slope angle for the existence of the fixed points:

1. ${}^{lc}Z^*$. A *sufficient* condition on the slope angle for the existence of the limit cycle associated with the fixed point ${}^{lc}Z^*$ is $\alpha > \frac{\pi}{n}$. The condition is sufficient since, for steep slopes and any measure of angular velocity, only the limit cycle exists. In other words, the map is linear with positive slope less than one, for all Z, and intersects the identity line $P(Z) = Z$ only once at some positive measure of angular velocity, the limit cycle fixed point. The map graph in Figure 8(d) shows that only the limit cycle exists for $\alpha > \frac{\pi}{n}$.

2. ${}^{stp}Z^* = 0$. A *necessary* and *sufficient* condition for the existence of the stopped position associated with the fixed point ${}^{stp}Z^*$ is $\alpha \leq \frac{\pi}{n}$. This condition is necessary since the return map does not intersect the identity line at $Z = 0$ for $\alpha > \frac{\pi}{n}$ and, thus, the wheel can never approach the stopped position. The map graph of the map in Figure 8(d) shows that the stopped condition does not exist for $\alpha > \frac{\pi}{n}$. For $\alpha \leq \frac{\pi}{n}$, the map can intersect the identity line at $Z = 0$. The map graphs in Figure 8(a)-(c) show how the stopped condition can exist for $\alpha \leq \frac{\pi}{n}$.

There is an additional restriction, however, on the slope angle that, together with that above, completely specifies the existence of the limit cycle. The necessary condition for the existence of the limit cycle corresponding to the fixed point ${}^{lc}Z^*$ can be derived as follows. For a limit cycle to exist, the wheel must be able to make it past the vertical position in the downhill direction repeatedly after each collision; *i.e.*, the limit cycle measure of angular velocity must be greater than or equal to the angular velocity just after a collision required to reach the vertical in infinite time:

$$^{lc}Z^* \geq {}^{dn}Z. \tag{21}$$

Referring to the definitions of $^{lc}Z^*$ in Equation (19) and ^{dn}Z in Equation (12) this inequality can be rewritten as a criterion relating slope angle α, collision parameter μ, and number of spokes n:

$$g(\alpha, n, \mu) \equiv 1 - \cos\frac{\pi}{n}\cos\alpha - \frac{1+\mu^2}{1-\mu^2}\sin\frac{\pi}{n}\sin\alpha \leq 0. \tag{22}$$

Taking α as a function of n and μ, this inequality requires that

$$\alpha \geq \alpha_c \tag{23}$$

where α_c is a solution to $g(\alpha, n, \mu) = 0$. Figure 8(a)-(b) show a graph of the return map for $\alpha < \alpha_c$ and $\alpha = \alpha_c$. A graph of $g(\alpha, n, \mu)$ versus α for fixed n and μ verifies that $\alpha > \alpha_c$ satisfies the inequality in Equation 22(see Figure 9(a)). Figure 9(b) shows the dependence of the critical angles on the number of spokes, n, and μ and also that the critical angle obeys the inequality $\alpha_c \leq \frac{\pi}{n}$. A necessary condition, then, for the existence of the limit cycle corresponding to the fixed point $^{lc}Z^* > 0$ is $\alpha > \alpha_c$.

In summary, the necessary and sufficient conditions on slope angle for the existence of the fixed points of P are:

1. $^{lc}Z^*$: $\alpha_c \leq \alpha \leq \frac{\pi}{2}$
2. $^{stp}Z^*$: $0 \leq \alpha \leq \frac{\pi}{n}$.

As α is varied, then, the number and type of fixed points change. The appearance and disappearance of the fixed points as the slope angle α is varied cannot be classified according to the classical theory of bifurcation of scalar maps due to the discontinuity in the Poincaré map. The fixed points are shown as a function of α in Figure 9(c) for fixed μ and n.

6.2 Basins of Attraction for the Fixed Points

We quantify here the domains of attraction for the fixed points within each of the three slope intervals. So far, we have determined within each slope interval which fixed points exist. We also know that, for all initial conditions, the wheel always enters into a limit cycle for steep slopes, $\alpha > \frac{\pi}{n}$. Any initial condition is attracted to limit cycle motion for this slope range since the map P is linear, with slope less than one, continuous for all Z, and thus intersects the identity line only once at some non-zero measure of angular velocity. The domains of attraction for the fixed points within the remaining two slope intervals remains to be prescribed because of the piecewise linearity of the map and the possibility of the wheel eventually stopping in the vertical position after one or more collisions.

The values of initial measure of angular velocity attracted to the fixed points for shallow and intermediate slopes can be completely specified by considering two situations regarding the measure of angular velocity. We describe the two situations first and then follow with a detailed analysis of each.

First, for rolling uphill or downhill on shallow or intermediate slopes, it is possible that the wheel starts with a velocity just after collision that eventually leaves the wheel, after one or more collisions, with the critical velocities after collision for reaching the vertical position in infinite time, ^{up}Z or ^{dn}Z. For such initial conditions, limit cycles and the stopped position cannot exist. The initial conditions that eventually leave the wheel in the vertical position can be found as three different monotonic infinite sequences of angular velocities after collision where each term in the sequence depends on the wheel parameters.

Second, for intermediate slopes only, the wheel can do one of three things: reach the vertical position, come to rest on two spokes, or approach the limit cycle. Initial angular velocities which are

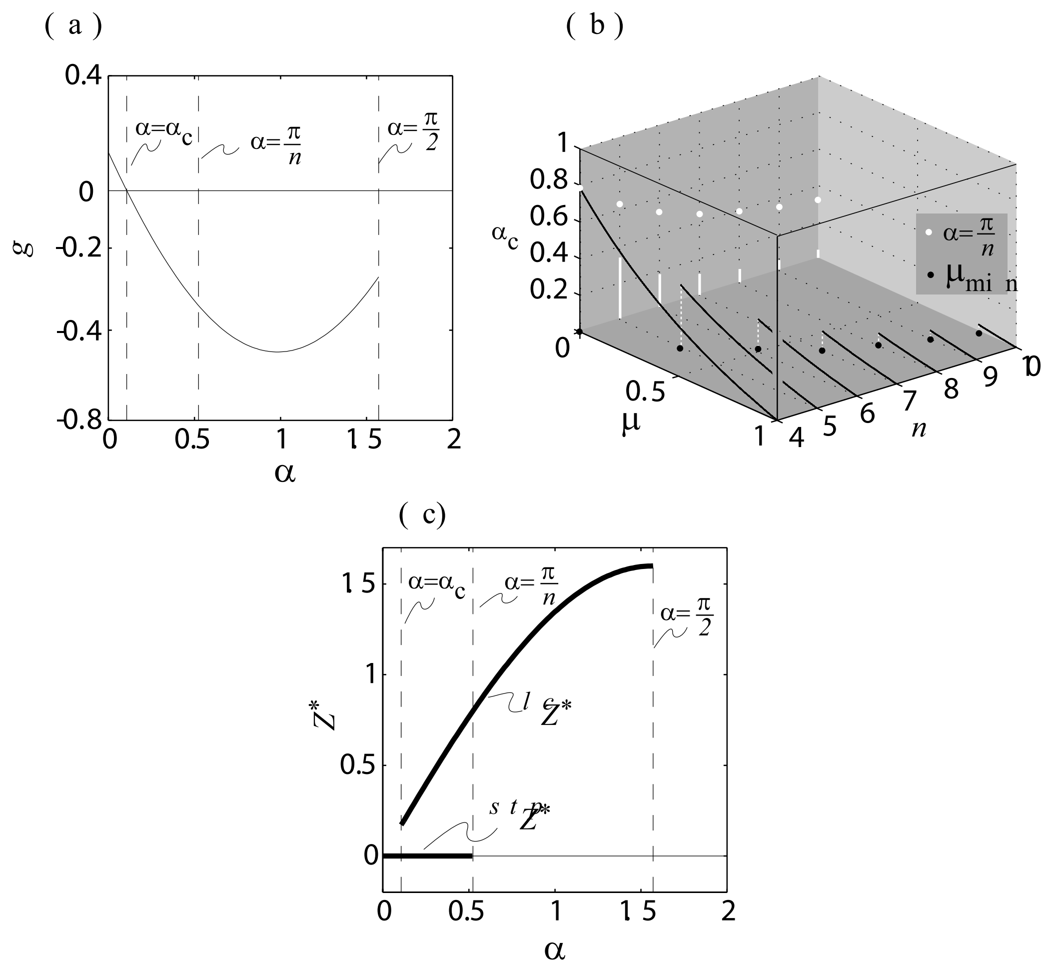

Figure 9: (a) A graph of $g(\alpha, n, \mu)$ versus α for $\mu = \frac{2}{3}$ and $n = 6$. The function g is less than zero for $\alpha > \alpha_c$. If $g < 0$, then limit cycles can exist. (b) The critical slope angle, α_c, is shown as function of n and μ. The white vertical dashed lines are aids to help visualize the curves. The curves are shown projected onto the $n - \alpha_c$ plane in solid white to show the range of critical slope angles for each n. Also shown on the same coordinate plane is $\alpha = \frac{\pi}{n}$, the upper bound on slope angle for the stopped position to exist; note that $\alpha \leq \frac{\pi}{n}$ for all n. The minimum damping coefficient, $\mu_{min} = \cos(\frac{2\pi}{n})$, is shown as a function of n on the $\mu - n$ plane. (c) The fixed points of P are graphed as a function of slope angle for $\mu = \frac{2}{3}$ and $n = 6$. The graph shows that only the stopped position is available as a limiting state for $\alpha < \alpha_c$, both the stopped position and the limit cycle are available as limiting states for $\alpha_c \leq \alpha \leq \frac{\pi}{n}$, and only the limit cycle is available as a limiting state for $\alpha > \frac{\pi}{n}$. This plot is a projection of the 3D plot in Figure 12 onto the $\alpha - Z^*$ plane.

attracted to the limit cycle and those which are attracted to the stopped position are organized into alternating 'patches' of initial angular velocity after collisions; *i.e.*, alternating subsets of the domain of the map P that we call *basins of attraction*. The 'patches' can be visualized as alternating line segments along the horizontal axis of the graph of $P(Z)$. The boundaries of the 'patches' are defined by the critical angular velocities after collision for reaching the vertical in infinite time and the terms in the infinite sequences described above that eventually get mapped to the vertical position.

6.2.1 Infinite Sequences of Angular Velocity After Collision

We derive here the three very special and improbable infinite sequences of the after-collision angular rate that leave the wheel eventually in the vertical position. Each of the sequences is constructed as follows. First, we find the first point in the sequence as the measure of angular velocity after one collision such that, after the next collision, the wheel reaches the vertical in infinite time. Then, we find the second point as the measure of angular velocity such that the after a collision the wheel emerges with the measure of angular velocity that is the first point in the sequence and so on up to the m_{th} measure of angular velocity in the sequence. We also determine the complete conditions for the existence of each sequence. For each of the sequences to exist, the necessary condition is that $\alpha \leq \frac{\pi}{n}$; otherwise, the vertical position does not exist.

1. The first sequence of points is defined for initially rolling downhill with greater angular velocity after collision than that required to eventually stop in the vertical position. There exists a monotonically increasing infinite sequence of measures of angular velocity after collision, ${}^{dn}Z_m > {}^{dn}Z > 0$ for $m = 1, 2, 3, \ldots$, such that if the wheel starts with any measure of angular velocity in the sequence, the wheel will eventually stop in the vertical position in the downhill direction after a finite number of collisions; *i.e.*, each measure of angular velocity ${}^{dn}Z_m$ gets mapped eventually by the return map P to ${}^{dn}Z$ in m iterations, $P^m({}^{dn}Z_m) = {}^{dn}Z$. The first point in the sequence, ${}^{dn}Z_1$, the point that gets mapped to ${}^{dn}Z$ after one collision, is found by solving

$$\begin{aligned} {}^{dn}Z &= P({}^{dn}Z_1) \quad \text{or} & (24)\\ {}^{dn}Z_1 &= \frac{{}^{dn}Z}{\mu^2} - 4\sin\alpha\sin\frac{\pi}{n}. & (25) \end{aligned}$$

   Then, similarly,

$$\begin{aligned} {}^{dn}Z_1 &= P({}^{dn}Z_2) \quad \text{or} & (26)\\ {}^{dn}Z_2 &= \frac{{}^{dn}Z_1}{\mu^2} - 4\sin\alpha\sin\frac{\pi}{n}(1 + \frac{1}{\mu^2}) & \\ &= \frac{{}^{dn}Z}{(\mu^2)^2} - 4\sin\alpha\sin\frac{\pi}{n}(1 + \frac{1}{\mu^2}). & (27) \end{aligned}$$

   Next,

$${}^{dn}Z_3 = \frac{{}^{dn}Z}{(\mu^2)^3} - 4\sin\alpha\sin\frac{\pi}{n}(1 + \frac{1}{\mu^2} + \frac{1}{(\mu^2)^2}) \tag{28}$$

   and so on until

$$\begin{aligned} {}^{dn}Z_m &= \frac{{}^{dn}Z}{\mu^{2m}} - 4\sin\alpha\sin\frac{\pi}{n}(1 + \frac{1}{\mu^2} + \frac{1}{(\mu^2)^2} + \cdots + \frac{1}{\mu^{2(m-1)}}) & \\ &= \frac{{}^{dn}Z}{\mu^{2m}} - 4\sin\alpha\sin\frac{\pi}{n}\sum_{k=1}^{m}\frac{1}{\mu^{2(k-1)}}. & (29) \end{aligned}$$

   The other two infinite sequences below are derived similarly. Summing the series yields

$${}^{dn}Z_m = \frac{{}^{dn}Z}{\mu^{2m}} - 4\sin\alpha\sin\frac{\pi}{n}\frac{\mu^{2m}-1}{\mu^2-1}\frac{\mu^2}{\mu^{2m}}. \tag{30}$$

The existence of this sequence requires that each angular velocity after collision in the sequence be greater than the angular velocity after collision that is necessary for the wheel to eventually stop in the vertical position; *i.e.*, the inequality ${}^{dn}Z_m > {}^{dn}Z > 0$ holds. This requirement yields a necessary and sufficient condition for the existence of the sequence,

$$\begin{aligned} g(\alpha, n, \mu) &> 0 \quad \text{or} \\ \alpha &< \alpha_c \end{aligned} \tag{31}$$

where the function g and critical angle α_c are defined in Equations (22) and (23). Thus, the slope angle must be nearly flat for the sequence to exist and so, correspondingly, no limit cycles exist. The wheel can only come to rest eventually.

2. The second sequence of points is defined for initially rolling uphill with angular velocity after collision greater in magnitude than that required to eventually stop in the vertical position in the uphill direction. There exists a monotonically decreasing sequence of the measures of angular velocity after collision, ${}^{up}Z_m < {}^{up}Z < 0$, $m = 1, 2, 3, \ldots$, such that if the wheel starts with any angular velocity in the sequence, the wheel will eventually stop in the vertical position in the uphill direction after a finite number of collisions; *i.e.*, each measure of angular velocity ${}^{up}Z_m < {}^{up}Z < 0$ gets mapped eventually by the map P to ${}^{up}Z$ in m iterations, $P^m({}^{up}Z_m) = {}^{up}Z$. Deriving this sequence as above for the first one, we obtain

$$ {}^{up}Z_m = \frac{{}^{up}Z}{\mu^{2m}} - 4 \sin\alpha \sin\frac{\pi}{n}\frac{\mu^{2m}-1}{\mu^2-1}\frac{\mu^2}{\mu^{2m}}. \tag{32}$$

The existence of this sequence requires that each angular velocity after collision in the sequence be greater in magnitude than the angular velocity after collision necessary for the wheel to eventually stop in the vertical position; *i.e.*, the inequality ${}^{up}Z_m < {}^{up}Z < 0$ holds. This requirement leads to a necessary condition for the existence of the sequence,

$$1 - \cos\frac{\pi}{n}\cos\alpha + \frac{1+\mu^2}{1-\mu^2}\sin\frac{\pi}{n}\sin\alpha > 0. \tag{33}$$

This equality holds for any slope angle, $0 \le \alpha \le \frac{\pi}{2}$. But, we already have the more restrictive condition for the sequence to exist, $0 \le \alpha \le \frac{\pi}{n}$, so that the vertical position is attainable. This condition is necessary and sufficient. Thus, this sequence exists for rolling on flat surfaces to intermediate slopes. Both the stopped position and limit cycles exist in this regime as well.

3. The third sequence of points is defined for initially rolling uphill with angular velocity after collision greater in magnitude than that required to eventually stop in the vertical position. The wheel, however, eventually reverses direction after one or more uphill collisions and then makes one downhill collision before stopping in the vertical position in the downhill direction in infinite time.

   To begin, there exists a measure of angular velocity after collision, ${}^{up}\bar{Z} = -(\frac{{}^{dn}Z}{\mu^2})$, ${}^{up}Z < {}^{up}\bar{Z} < 0$, such that the wheel fails to make it past the vertical position in the uphill direction, reverses direction, makes one collision in the downhill direction and eventually stops in the vertical position; *i.e.*, ${}^{up}\bar{Z}$ gets mapped by P in one iteration to ${}^{dn}Z$. If ${}^{up}\bar{Z}$ exists, then there exists a monotonically decreasing sequence of angular velocities after collision, ${}^{up}\bar{Z}_m < {}^{up}Z < 0$, such that if the wheel starts with any angular velocity in the sequence, the wheel will eventually stop in the vertical position in the downhill direction; *i.e.*, each measure of angular velocity ${}^{up}\bar{Z}_m$, ${}^{up}\bar{Z}_m < {}^{up}Z < 0$ gets mapped eventually by P to ${}^{up}\bar{Z}$ in m iterations and then to ${}^{dn}Z$ in one iteration, $P^{m+1}({}^{up}\bar{Z}_m) = {}^{dn}Z$. Deriving the sequence again as for the first one, we obtain

$$ {}^{up}\bar{Z}_m = -\frac{{}^{dn}Z}{\mu^{2(m+1)}} - 4 \sin\alpha \sin\frac{\pi}{n}\frac{\mu^{2m}-1}{\mu^2-1}\frac{\mu^2}{\mu^{2m}}. \tag{34}$$

The existence of this sequence requires that the inequalities ${}^{up}Z < {}^{up}\bar{Z} < 0$ and ${}^{up}\bar{Z}_m < {}^{up}Z < 0$ hold. Both of these inequalities yield the condition

$$\begin{aligned} g(\alpha, n, \mu) &< 0 \ \text{ or} \\ \alpha &> \alpha_c. \end{aligned} \tag{35}$$

Thus, a necessary and sufficient condition for the sequence to exist is that the slope be intermediate in size; i.e., $\alpha_c < \alpha < \frac{\pi}{n}$. Correspondingly, both coming to rest and the limit cycle exist in this slope regime.

The existence of these sequences and critical measures of angular velocity, is summarized in Table 1.

Table 1: The existence of the critical angular velocities and sequences of angular velocities for $0 \leq \alpha \leq \frac{\pi}{2}$. The existence of the points and sequences in each slope regime are noted by asterisks in each column of the table.

	Measures of Angular Velocity					
Slope Angle α	${}^{up}Z$	${}^{up}Z_m$	${}^{dn}Z$	${}^{dn}Z_m$	${}^{up}\bar{Z}$	${}^{up}\bar{Z}_m$
$0 \leq \alpha < \alpha_c$	*	*	*	*		
$\alpha = \alpha_c$	*		*			
$\alpha_c < \alpha < \frac{\pi}{n}$	*	*	*		*	*
$\alpha = \frac{\pi}{n}$	*	*				
$\frac{\pi}{n} < \alpha \leq \frac{\pi}{2}$						

6.2.2 Alternating Basins of Attraction for Intermediate Slopes

We define here alternating basins of attraction of initial angular speed after collision that exist only for intermediate slope angles, $\alpha_c < \alpha \leq \frac{\pi}{n}$.

1. In this slope range, if the wheel starts off downhill, it has one of three initial energies:
   (a) critical energy for reaching the vertical in infinite time (denoted by Down$\rightarrow$ Vertical),
   (b) less than the energy needed to pass the vertical in the downhill direction so that it approaches the stopped position by rocking back and forth on two spokes (denoted by Down$\rightarrow$ Rock $\rightarrow$ Stop), or
   (c) more than the energy needed to pass the vertical so that it approaches the limit cycle from above or below (denoted by Down$\xrightarrow{-}$ Limit Cycle or Down$\xrightarrow{+}$ Limit Cycle, respectively).
2. If the wheel starts uphill, it has one of three initial energies:
   (a) critical energy for reaching the vertical in infinite time(denoted by Up$\rightarrow$ Vertical),
   (b) energy such that the initial angular velocity is in one of the critical sequences and it eventually stops in the vertical position, or
   (c) enough energy to pass the vertical in the uphill direction but, after one or more collisions, loses so much energy in the collision(s) that, eventually, it cannot make it past the vertical, reverses direction and starts downhill. The subsequent behavior after the wheel reverses direction is determined by the energy of the wheel after the last collision before reversing direction. If the wheel has too little energy after the last collision before reversing direction, it makes one downhill collision, cannot make it past the vertical in the downhill direction, rocks back and forth between two spokes, and approaches the stopped position (denoted by Up$\rightarrow$ Rock $\rightarrow$ Stop). If the wheel has sufficient energy after the last collision before reversing direction, it has enough energy to pass the vertical in the downhill direction, increases in angular velocity and approaches the limit cycle from below (denoted by Up$\rightarrow$ Down $\xrightarrow{+}$ Limit Cycle).

For intermediate slopes, whether starting off downhill or uphill, the initial energy of the wheel, then, predetermines if the wheel will reach the vertical position, the limit cycle, or the stopped position. If the wheel starts with the measure of angular velocity ${}^{dn}Z$ and ${}^{up}Z$ or one of the measures of angular velocity in the sequences ${}^{up}Z_m$ or ${}^{up}\bar{Z}_m$, the wheel will eventually stop in the vertical position.

Similarly well defined sets of initial measure of angular velocity eventually approach either the limit cycle or the stopped condition, exclusively. As we have noted, the initial angular velocities that are attracted to the limit cycle and those which are attracted to the stopped position are organized into alternating 'patches' or basins of attraction. If the angular velocities in a given basin of attraction get mapped to the limit cycle, the adjacent basin of initial conditions gets mapped to the stopped condition, and so on, for each succeeding 'patch', alternating in this way. The boundaries of the basins are formed by the critical measures of angular velocity, ${}^{dn}Z$ and ${}^{up}Z$, and the terms of the second and third sequences we have just defined, ${}^{up}Z_m$ and ${}^{up}\bar{Z}_m$.

In order to define the basins of attraction, we need first to order the critical points and the terms of the second and third sequences. The critical points and the terms of the sequences are ordered as follows:

$$ {}^{up}Z_m < {}^{up}\bar{Z}_m < {}^{up}Z < {}^{up}\bar{Z} < 0 \tag{36} $$

and

$$ {}^{up}Z_{m+1} < {}^{up}\bar{Z}_{m+1} < {}^{up}Z_m. \tag{37} $$

(It is trivial to prove that these inequalities hold for $\alpha_c < \alpha < \frac{\pi}{n}$.)

Now that the important points are ordered, which basins are attracted to the limit cycle and which are attracted to the stopped position can be determined visually by examining graphs of the Poincaré map. For example, reconsider the map of Figure 7 in Figure 10 with restrictions on the measure of angular velocity added for determining which fixed points exist.

Thus, generalizing from the special case illustrated in Figure 10 for $\alpha_c < \alpha < \frac{\pi}{n}$, we state without proof: the basins of attraction for the limit cycle are

$$ Z > {}^{dn}Z, \quad {}^{up}Z < Z < {}^{up}\bar{Z}, \quad \text{and} \quad {}^{up}Z_m < Z < {}^{up}\bar{Z}_m, \tag{38} $$

and the basins of attraction for the stopped position are

$$ {}^{up}\bar{Z} < Z < {}^{dn}Z, \quad {}^{up}\bar{Z}_1 < Z < {}^{up}Z, \quad \text{and} \quad {}^{up}\bar{Z}_{m+1} < Z < {}^{up}Z_m. \tag{39} $$

The basins of attraction for the fixed fixed points given intermediate slope angles, $\alpha_c < \alpha < \frac{\pi}{n}$, are summarized in Table 2.

Table 2: The basins of attraction for the fixed points corresponding to the limit cycle and the stopped position with intermediate slope angle, $\alpha_c < \alpha < \frac{\pi}{n}$, are noted by asterisks in each row of the table.

	Fixed Points	
Measure of Angular Velocity	${}^{lc}Z^*$	${}^{stp}Z^*$
${}^{up}\bar{Z}_{m+1} < Z < {}^{up}Z_m$		*
${}^{up}Z_m < Z < {}^{up}\bar{Z}_m$	*	
${}^{up}\bar{Z}_1 < Z < {}^{up}Z$		*
${}^{up}Z < Z < {}^{up}\bar{Z}$	*	
${}^{up}\bar{Z} < Z < {}^{dn}Z$		*
$Z > {}^{dn}Z$	*	

Given an initial measure of angular velocity for starting off rolling uphill, the number of collisions before reversing direction are as follows:

1. for ${}^{up}\bar{Z}_{m+1} < Z < {}^{up}Z_m$, $m+1$ collisions occur before the wheel reverses direction and converges to ${}^{stp}Z^*$.

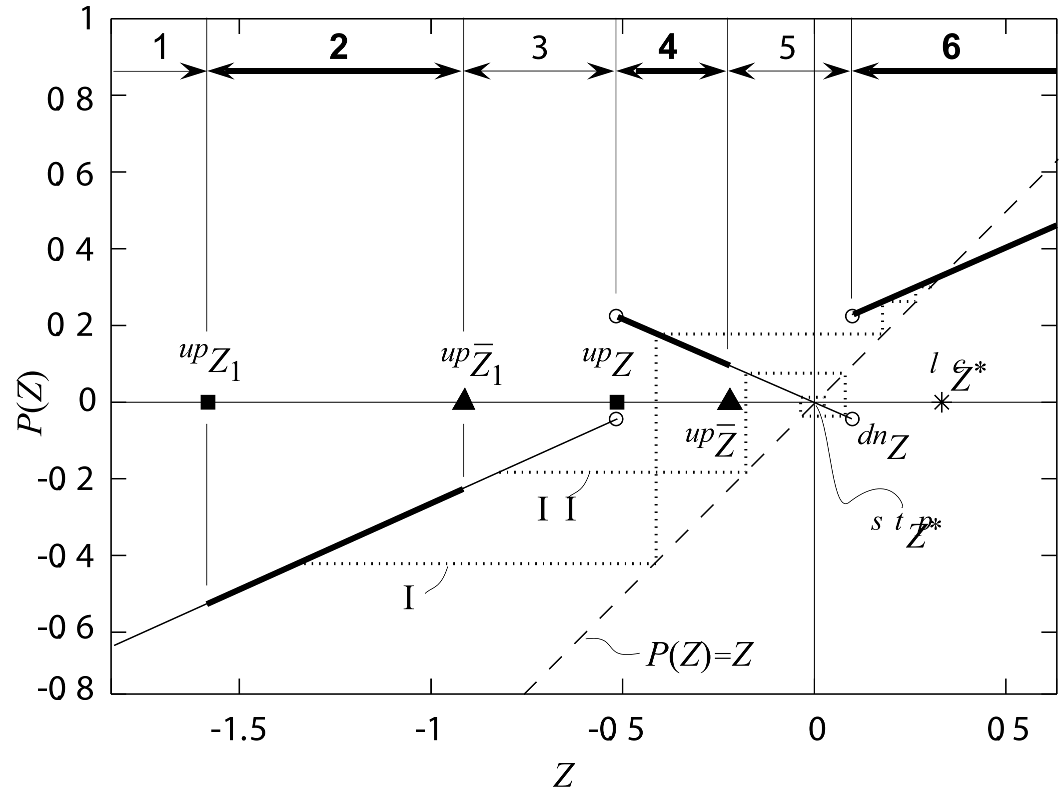

Figure 10: Again, the graph of the Poincarè map with $\mu = \frac{2}{3}$, $n = 6$, and $\alpha = \frac{\pi}{15} < \frac{\pi}{6}$. The critical measures of angular velocity, the fixed points, and the sequences $^{up}Z_m$ and $^{up}\bar{Z}_m$ are marked on the graph up to $m = 1$ for the given wheel parameters. The basins of initial measure of angular velocity attracted to the limit cycle are marked on the graph with bold line segments to differentiate them from those attracted to the stopped position. Six representative basins of attraction are labeled on the graph. Initial conditions in the intervals (1), $^{up}\bar{Z}_2 < Z < {}^{up}Z_1$, (3), $^{up}\bar{Z}_1 < Z < {}^{up}Z$, and (5), $^{up}\bar{Z} < Z < {}^{dn}Z$ get mapped to the stopped condition corresponding to the fixed point $^{stp}Z^*$. Initial conditions in the intervals (2), $^{up}Z_1 < Z < {}^{up}\bar{Z}_1$, (4), $^{up}Z < Z < {}^{up}\bar{Z}$, and (6), $^{dn}Z < Z < \infty$ get mapped to the limit cycle corresponding to the fixed point $^{lc}Z^*$. The orbit labeled I starts in interval (2) and converges to the limit cycle fixed point. The orbit labeled II starts in interval (3) and converges to the zero fixed point.

2. for $^{up}Z_m < Z < {}^{up}\bar{Z}_m$, m collisions occur before the wheel reverses direction and converges to $^{lc}Z^*$.

6.3 Special Cases

1. $\alpha = \alpha_c$:

   (a) The limit cycle angular velocity is equal to the angular velocity after collision in the downhill direction for stopping in the vertical position in infinite time; *i.e.*, $^{lc}Z^* = {}^{dn}Z$. Convergence to the limit cycle only occurs for $Z > {}^{lc}Z^* = {}^{dn}Z$.

   (b) If $Z < {}^{lc}Z^* = {}^{dn}Z$, the wheel approaches the stopped position.

2. $\alpha = \frac{\pi}{n}$:

   (a) The wheel is oriented at the vertical position $\theta = -\alpha$ at each collision. The critical measures of angular velocity are $^{dn}Z = 0$ and $^{up}Z = -4\sin^2\frac{\pi}{n}$.

(b) If $Z > 0$, the wheel will roll down the slope. If $Z = 0$, a small positive disturbance will cause the wheel to fall downhill.

(c) If ${}^{up}Z < Z < 0$, the wheel makes a collision instantaneously with the slope in the uphill direction but loses so much energy in collision that it cannot reach the next vertical position, falls back down the slope, and converges to a limit cycle.

(d) If the angular velocity just after collision is $Z < {}^{up}Z < 0$, the wheel makes a collision instantaneously with the slope in the uphill direction and makes one or more collisions in the uphill direction before reversing direction and converging to a limit cycle.

(e) The vertical position (balanced at rest unstably on one spoke) and the stopped position (at rest stably on two spokes) are indistinguishable. The only way, then, in which the stopped condition (corresponding to the fixed point ${}^{stp}Z^* = {}^{dn}Z = 0$) can exist is if the wheel stays at rest, $Z = 0$.

3. $\mu \leq 0$:

(a) If $\mu = 0$, then $\alpha_c = \frac{\pi}{n}$. When $\mu = 0$, $\lambda^2 = \frac{1}{1-\cos(\frac{2\pi}{n})} \leq 1$; *i.e.*, either $\lambda^2 = \frac{2}{3}$ and $n = 3$ OR $\lambda^2 = 1$ (zero moment of inertia) and $n = 4$.

(b) If $\mu = 0$, the angular rate after collision equals zero, according to the collision condition, Equation (9), and, thus, for any initial conditions, only the stopped position exists. The wheel either rotates past the vertical or does not and then comes to a complete stop after one collision in finite time, (not by rocking back and forth on two spokes and coming to a stop after infinite collisions in finite time). We denoted this behavior previously by Up$\rightarrow$ Stop or Down$\rightarrow$ Stop. These behaviors only exist, then, for $\alpha \leq \frac{\pi}{n}$.

(c) If $n = 3$ and $\frac{2}{3} < \lambda^2 \leq 1$, then $-0.5 \leq \mu < 0$. For $\mu < 0$, the wheel would instantaneously reverse direction after a collision *and* slow down, leading to an infinite sequence of collisions in *zero* time with *no* motion. That is, the entire wheel stops dead, not just the tip of the colliding spoke.

(d) To summarize:

i. if $n = 4$ and $\lambda^2 = 1$ (zero moment of inertia), then $\mu = 0$ and

ii. if $n = 3$ and $\frac{2}{3} \leq \lambda^2 \leq 1$, then $-0.5 \leq \mu \leq 0$.

6.4 Summary of the Existence Criteria and Basins of Attraction for Fixed Points

In Table 3, we summarize the necessary and sufficient conditions on slope angle, α, and measure of angular velocity after collision, Z, that specify which of the fixed points will arise. We display the information tabulated in Table 3 using two representations. First, in Figure 11, to display the existence criteria for the fixed points and their dependence on initial conditions and parameters, we code the return maps for fixed n and μ but with a variety of slope angles to show which initial conditions are attracted to the limit cycle and those which are attracted to the stopped position. Second, in Figure 12, we show the dependence of the basins of attraction on slope angle for fixed n and μ.

For Figure 11, we obtain the curves bounding the regions that mark the basins of attraction as follows:

1. Two of the bounding curves are formed by the set of critical angular velocities for reaching the vertical in infinite time, ${}^{dn}Z(\alpha)$ and ${}^{up}Z(\alpha)$ for slope angle $0 \leq \alpha < \frac{\pi}{n}$. The curves can be found as functions of Z.

(a) In terms of the map P, we define the first curve as:

$$r({}^{dn}Z(\alpha)) \equiv P({}^{dn}Z(\alpha)) = \mu^2({}^{dn}Z(\alpha) + 2(\cos(\alpha - \frac{\pi}{n}) - \cos(\alpha + \frac{\pi}{n})) \tag{40}$$

Table 3: The dependence of the fixed points on the wheel parameters and the basins of attraction for the fixed points are summarized in the table. The critical angles, α_c and $\frac{\pi}{n}$, are functions of μ and n. The critical measures of the angular velocity are functions of α, μ, and n. For each slope range and all possible initial conditions, which fixed points arise are denoted by asterisks in the appropriate column.

		Fixed Points	
Slope Angle α	Measure of Angular Velocity	${}^{lc}Z^*$	${}^{stp}Z^*$
$0 \le \alpha < \alpha_c$	$Z \ne {}^{dn}Z, {}^{dn}Z_m, {}^{up}Z, {}^{up}Z_m$		*
$\alpha_c \le \alpha \le \frac{\pi}{n}$	${}^{up}\bar{Z}_{m+1} < Z < {}^{up}Z_m$		*
	${}^{up}Z_m < Z < {}^{up}Z_m$	*	
	${}^{up}Z_1 < Z < {}^{up}Z$		*
	${}^{up}Z < Z < {}^{up}Z$	*	
	${}^{up}Z < Z < {}^{dn}Z$		*
	$Z > {}^{dn}Z$	*	
$\frac{\pi}{n} < \alpha \le \frac{\pi}{2}$	all Z	*	

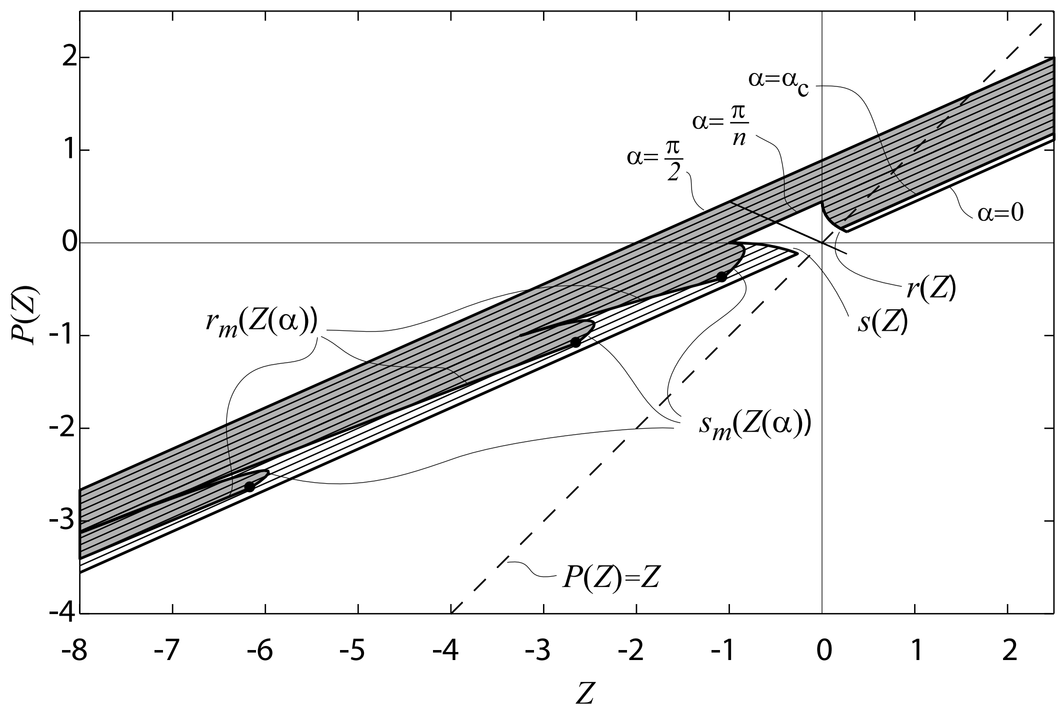

Figure 11: The return map for a variety of slope angles, $0 \le \alpha \le \frac{\pi}{2}$ and $\mu = \frac{2}{3}$ and $n = 6$. The initial values on the horizontal axis corresponding to the shaded region get mapped eventually to the limit cycle fixed point, ${}^{lc}Z^*$. All other initial conditions get mapped to the stopped position fixed point, ${}^{stp}Z^*$. The bounding curves demarcating the regions of attraction are noted on the diagram. Note that the maps are not coded for ${}^{up}Z < Z < {}^{dn}Z$ because for each α the map information is overlapping in this interval. The solid black dots are aids to visualize better the transition between the bounding curves r_m and s_m.

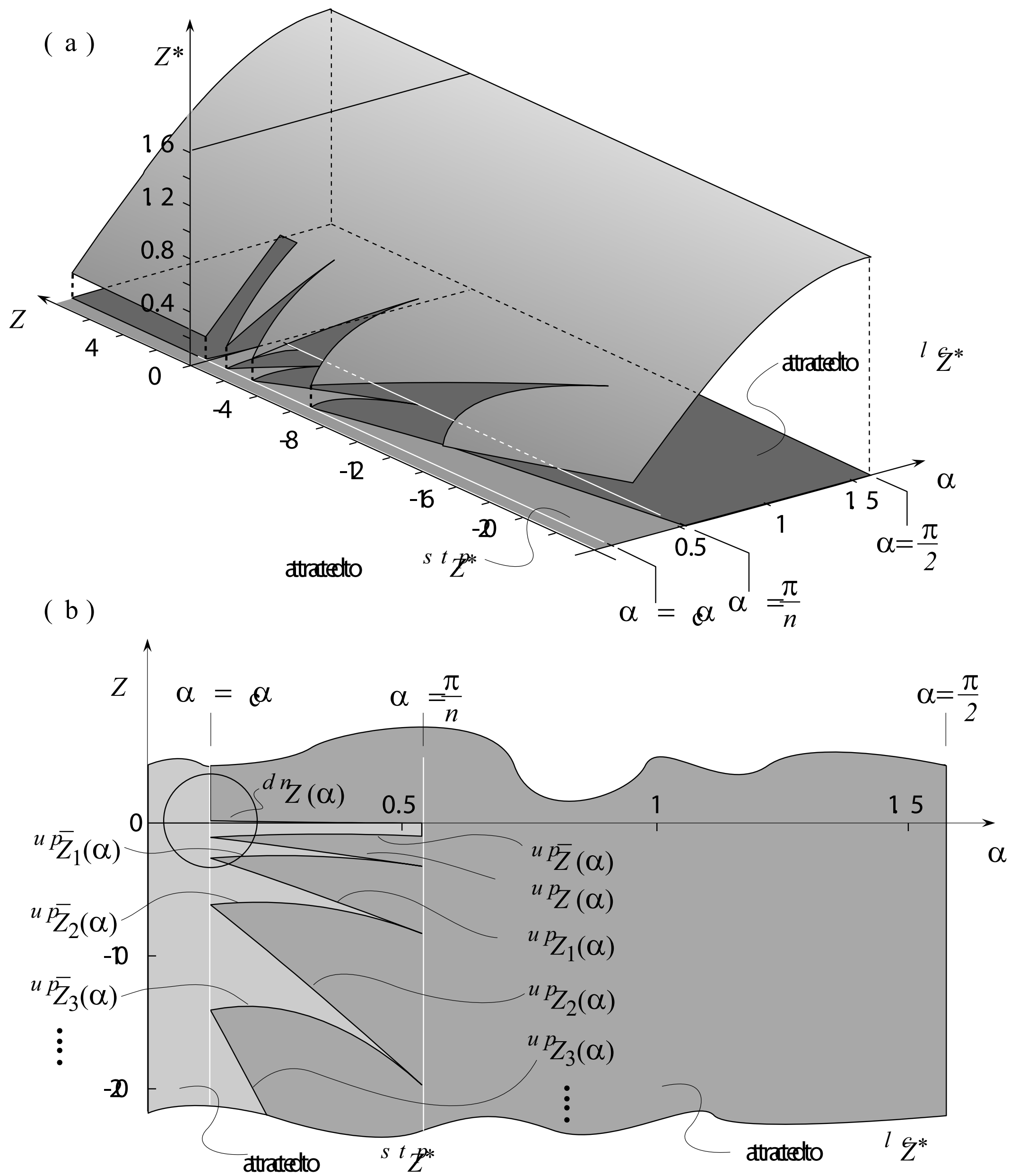

Figure 12: This figure displays the information summarized in Table 3 for a fixed number of spokes and damping coefficient, $n = 6$ and $\mu = \frac{2}{3}$. (a) For a given slope angle and initial condition, this 3D plot shows basins of attraction in the $\alpha - Z$ plane for the two fixed points. Initial values of Z falling in the light gray region for a given slope angle α are attracted to ${}^{stp}Z^*$ and those falling in the dark gray region are attracted to ${}^{lc}Z^*$. The values of Z^* for given (α, Z) are plotted along the vertical axis and form the 'toothed' surface shown; only a portion of the surface is shown. The solid white lines in this plot and in part(b) indicate the critical slope angles. The projection of this plot onto the $\alpha - Z^*$ plane gives the plot in Figure 9. The vertical dashed lines are aids to help visualize the surface. (b) This is a projection of the plot in (a) onto the $\alpha - Z$ plane. The curves that demarcate the boundaries of the basins of attraction are noted on the plot. This plot clearly shows the slope angle regimes for which only one or both of the fixed points exist. For the given n and μ, note that in the intermediate slope angle interval there is only a tiny region of downhill rolling initial conditions are attracted to ${}^{stp}Z^*$ (the region is barely visible inside the circle on the plot); all of the rest of the downhill initial conditions are attracted to the limit cycle.

$$= \quad 2\mu^2(1-\cos(\alpha+\frac{\pi}{n}))$$
$$= \quad 2\mu^2[1-\cos(\frac{2\pi}{n}-\arccos(1-\frac{{}^{dn}Z}{2}))]$$

where, referring to Equation (12), we have used $\alpha = \frac{\pi}{n} - \arccos(1-\frac{{}^{dn}Z}{2})$. Thus,

$$r(Z) = 2\mu^2[1-\cos(\frac{2\pi}{n}-\arccos(1-\frac{Z}{2}))], \quad 0 < Z < 2(1-\cos(\frac{\pi}{n})). \qquad (41)$$

(b) Similarly, we define the second curve to be:

$$s(Z) = 2\mu^2[\cos(\arccos(1+\frac{Z}{2})-\frac{2\pi}{n})-1], \quad -2(1-\cos(\frac{2\pi}{n})) < Z < -2(1-\cos(\frac{\pi}{n})). \qquad (42)$$

2. The remaining bounding curves are formed by sets of terms from the infinite sequences of angular velocities for intermediate slopes, ${}^{up}Z_m < {}^{up}Z$ and ${}^{up}\bar{Z}_m < {}^{up}Z$. For each m, the bounding curves can be found as functions of slope angle α for $\alpha_c < \alpha < \frac{\pi}{n}$ and ${}^{up}Z_m < Z < {}^{up}\bar{Z}_m$. (We use the shorthand notation $\mathrm{c}\alpha\ \mathrm{c}\frac{\pi}{n} = \cos\alpha\cos\frac{\pi}{n}$ and $\mathrm{s}\alpha\ \mathrm{s}\frac{\pi}{n} = \sin\alpha\sin\frac{\pi}{n}$.)

   (a) The first of the pair of curves for each m is:

$$r_m({}^{up}Z_m(\alpha)) \equiv P({}^{up}Z_m(\alpha)) = \qquad (43)$$
$$\frac{2}{(\mu^2-1)\mu^{2(m-1)}} \quad \left[\left(\mu^2-1\right)\left(1-\mathrm{c}\alpha\ \mathrm{c}\tfrac{\pi}{n}\right)-\left(3\mu^2-2\mu^{2m}-1\right)\left(\mathrm{s}\alpha\ \mathrm{s}\tfrac{\pi}{n}\right)\right]. \qquad (44)$$

   (b) The second of the pair of curves for each m is:

$$s_m({}^{up}\bar{Z}_m(\alpha)) \equiv P({}^{up}\bar{Z}_m(\alpha)) = \qquad (45)$$
$$\frac{2}{(\mu^2-1)\mu^{2m}} \quad \left[\left(\mu^2-1\right)\left(\mathrm{c}\alpha\ \mathrm{c}\tfrac{\pi}{n}-1\right)-\left(2\mu^4+\mu^2-2\mu^{2(m+1)}-1\right)\left(\mathrm{s}\alpha\ \mathrm{s}\tfrac{\pi}{n}\right)\right]. \qquad (46)$$

To visualize these bounding curves, we plot $r_m({}^{up}Z_m(\alpha))$ *vs.* ${}^{up}Z_m(\alpha)$ and $s_m({}^{up}\bar{Z}_m(\alpha))$ *vs.* ${}^{up}\bar{Z}_m(\alpha)$ for $m = 1, 2, \ldots$.

Finally, Figure 13 shows the basins of attraction for the fixed points in phase space for intermediate slope angles; the data is plotted in $(\theta, \dot{\theta})$ coordinates because it is much easier to visualize the trajectories shown.

7 Existence of Possible Wheel Behaviors and their Dependence on Initial Conditions

Different behaviors occur depending on whether the slope is very steep, intermediately steep, or nearly flat. Which behaviors arise in each of these slope intervals depends upon the initial conditions and physical parameters. The occurrences of each of the eleven behaviors, described above in Section 2.4, in the three slope intervals and for the two critical angles, α_c and $\alpha = \frac{\pi}{n}$, are indicated in Table 4.

The initial conditions for the angular velocity after collision can be greater than, less than, or equal to the critical angular velocities for reaching the vertical position in infinite time, ${}^{dn}Z$ or ${}^{up}Z$, or the fixed point angular velocities, ${}^{lc}Z^* > 0$ or ${}^{stp}Z^* = 0$. The possible behaviors for each slope interval and their dependence on initial conditions is summarized in five flowchart diagrams in Figure 14. The critical angular velocities ${}^{up}Z$ and ${}^{dn}Z$, the vertical position, and the stopped position do not exist for very steep slopes and limit cycles do not exist for nearly flat slopes.

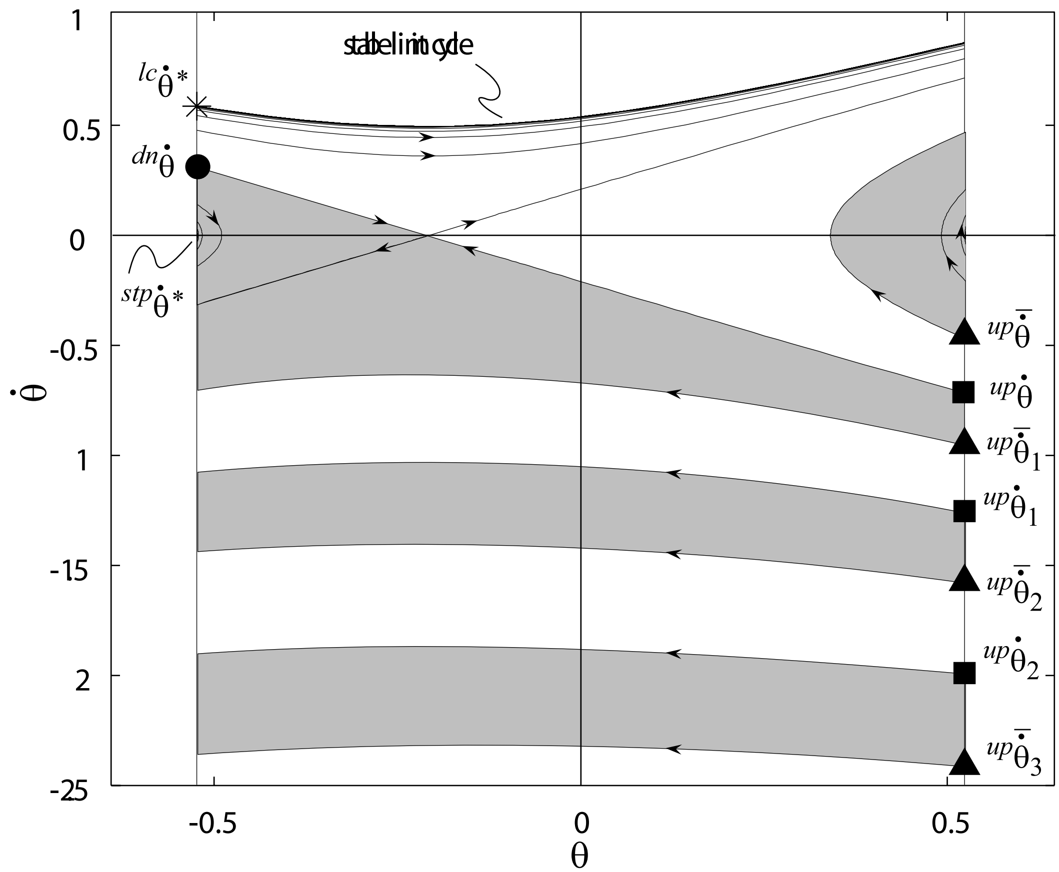

Figure 13: Basins of attraction for the fixed points in the $(\theta,\, \dot{\theta})$ phase space with $\alpha = \frac{\pi}{15}$, $n = 6$, and $\mu = \frac{2}{3}$. Initial conditions in the gray regions are attracted to $^{stp}Z^*$; all others are attracted to $^{lc}Z^*$. If the phase surface is bent around into a cylinder, the gray bands would form a 'jagged' ribbon spiraling up around the cylinder ending in the attracting region surrounding $^{stp}Z^*$.

Table 4: The dependence of the eleven possible behaviors on slope angle is indicated by an asterisk in each column.

		Slope Angle α				
Behavior		$0 \le \alpha < \alpha_c$	$\alpha = \alpha_c$	$\alpha_c < \alpha < \frac{\pi}{n}$	$\alpha = \frac{\pi}{n}$	$\frac{\pi}{n} < \alpha \le \frac{\pi}{2}$
1	Down$\xrightarrow{+}$ Limit Cycle			*	*	*
2	Down$\xrightarrow{-}$ Limit Cycle		*	*	*	*
3	Down$\to$ Rock $\to$ Stop	*				
4	Rock$\to$ Stop	*	*	*		
5	Up$\to$ Rock $\to$ Stop	*	*	*		
6	Up$\to$ Down $\xrightarrow{+}$ Limit Cycle			*	*	*
7	Down$\to$ Vertical	*	*	*		
8	Up$\to$ Vertical	*	*	*	*	
9	Up$\to$ Down $\to$ Vertical		*	*		
10	Up$\to$ Stop	*	*	*		
11	Down$\to$ Stop	*	*	*		

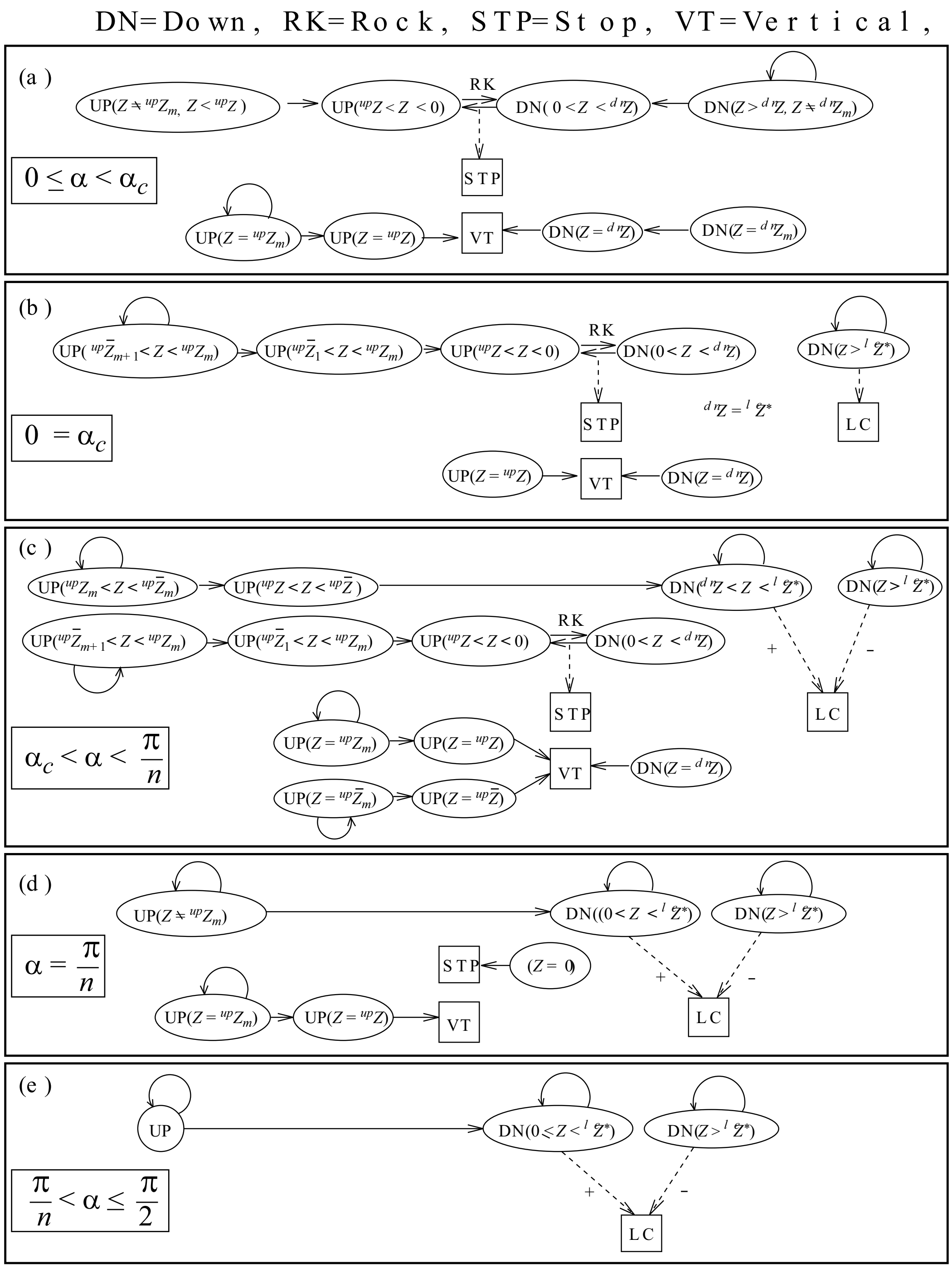

Figure 14: Five diagrams encapsulating the possible behaviors and their dependence on initial conditions for (a) $0 \leq \alpha < \alpha_c$, (b) $\alpha = \alpha_c$, (c) $\alpha_c < \alpha < \frac{\pi}{n}$, (d) $\alpha = \frac{\pi}{n}$, and (e) $\frac{\pi}{n} < \alpha \leq \frac{\pi}{2}$. The conventions used here are the same as in Figure 3 except that the plus(+) and minus(−) signs have been added to indicate increasing and decreasing speed, respectively, in reaching a limit cycle. Note that limit cycle motion does not exist for nearly flat slopes and neither the vertical position nor coming to rest on two spokes exists for very steep slopes.

8 Other Results

For shallow, intermediate, and steep slopes, we display some of the more interesting possible behaviors, out of a possible total of eleven behaviors, in the following plots:

(i) Poincaré map showing fixed points and characteristic stair-step diagrams.

(ii) Phase portrait showing the trajectories as the wheel approaches the fixed points.

Each plot displays the shorthand notation for the behavior displayed, the critical measures of angular velocity and sequences for reaching the vertical position in infinite time, the fixed points, the slope angle, the wheel parameters, and the initial conditions. For all cases, the non-dimensional collision parameter $\mu = \frac{2}{3}$ and the number of spokes is $n = 6$. For these given wheel parameters, the critical slope angle is $\alpha_c = 0.107$.

These graphs show how the existence of the fixed points depends on slope angle α and the initial measure angular velocity, $Z_0 \in \Sigma$. They also show how the wheel approaches the fixed points. The behaviors where the wheel reaches the vertical in infinite time or comes to a stop in one collision are not displayed; *i.e.*, behaviors 7-11, Down$\rightarrow$ Vertical, Up$\rightarrow$ Vertical, Up$\rightarrow$ Down$\rightarrow$ Vertical, Up$\rightarrow$ Stop, and Down$\rightarrow$ Stop. In addition, behavior 4 is the final part of behaviors 3 and 5 and, thus, is not displayed separately.

Figure 15 shows behaviors 3 and 5, Down$\rightarrow$ Rock $\rightarrow$ Stop and Up$\rightarrow$ Rock $\rightarrow$ Stop, respectively, for $0 \leq \alpha < \alpha_c$. Figure 16 shows behavior 6, Up$\rightarrow$ Down $\xrightarrow{+}$ Limit Cycle , for $\alpha_c \leq \alpha \leq \frac{\pi}{n}$. Figure 17 shows behaviors 1 and 2, Down$\xrightarrow{+}$ Limit Cycle and Down$\xrightarrow{-}$ Limit Cycle, respectively, for $\frac{\pi}{n} < \alpha \leq \frac{\pi}{2}$.

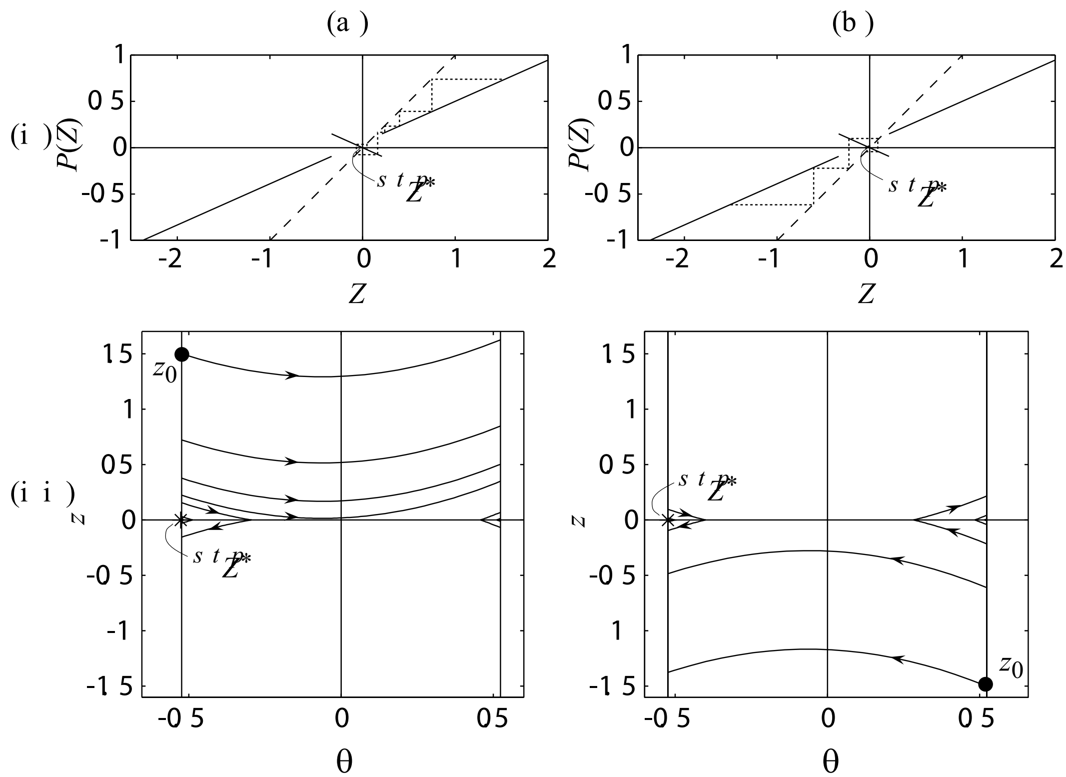

Figure 15: (a) The plots shown here characterize behavior 3, Down$\rightarrow$ Rock $\rightarrow$ Stop. The wheel parameters are $\mu = \frac{2}{3}$, $n = 6$, and $\alpha = \frac{\pi}{50}$. The initial condition is $Z_0 = 1.5$. The fixed point is ${}^{stp}Z^* = 0$. (b) The plots shown here characterize behavior 5, Up$\rightarrow$ Rock $\rightarrow$ Stop. The wheel parameters are $\mu = \frac{2}{3}$, $n = 6$, and $\alpha = \frac{\pi}{50}$. The initial condition is $= Z_0 = -1.5$. The fixed point is ${}^{stp}Z^* = 0$.

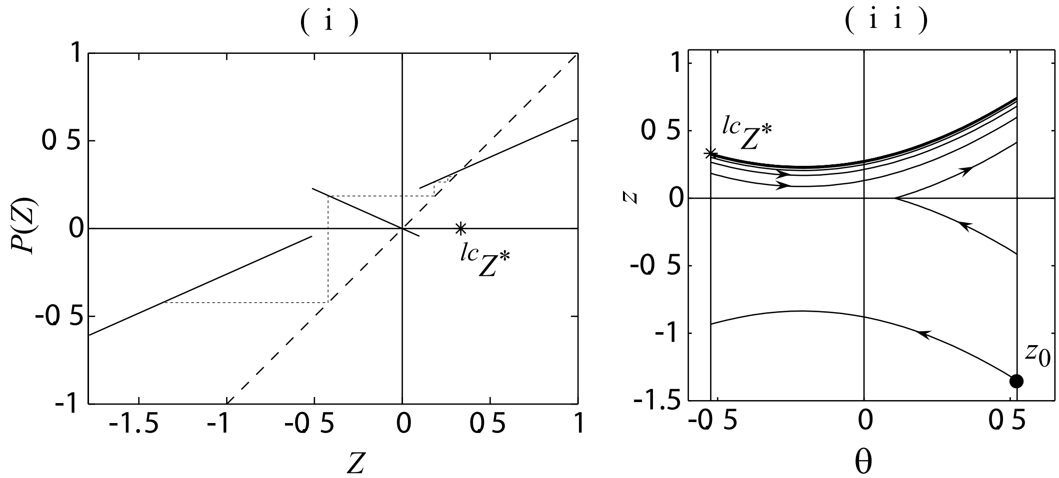

Figure 16: The plots shown here characterize behavior 6, Up$\rightarrow$ Down$\xrightarrow{+}$ Limit Cycle. The wheel parameters are $\mu = \frac{2}{3}$, $n = 6$, and $\alpha = \frac{\pi}{15}$. The initial condition is $Z_0 = -1.35$. For the given initial condition, the fixed point is $^{lc}Z^* = 0.3327$.

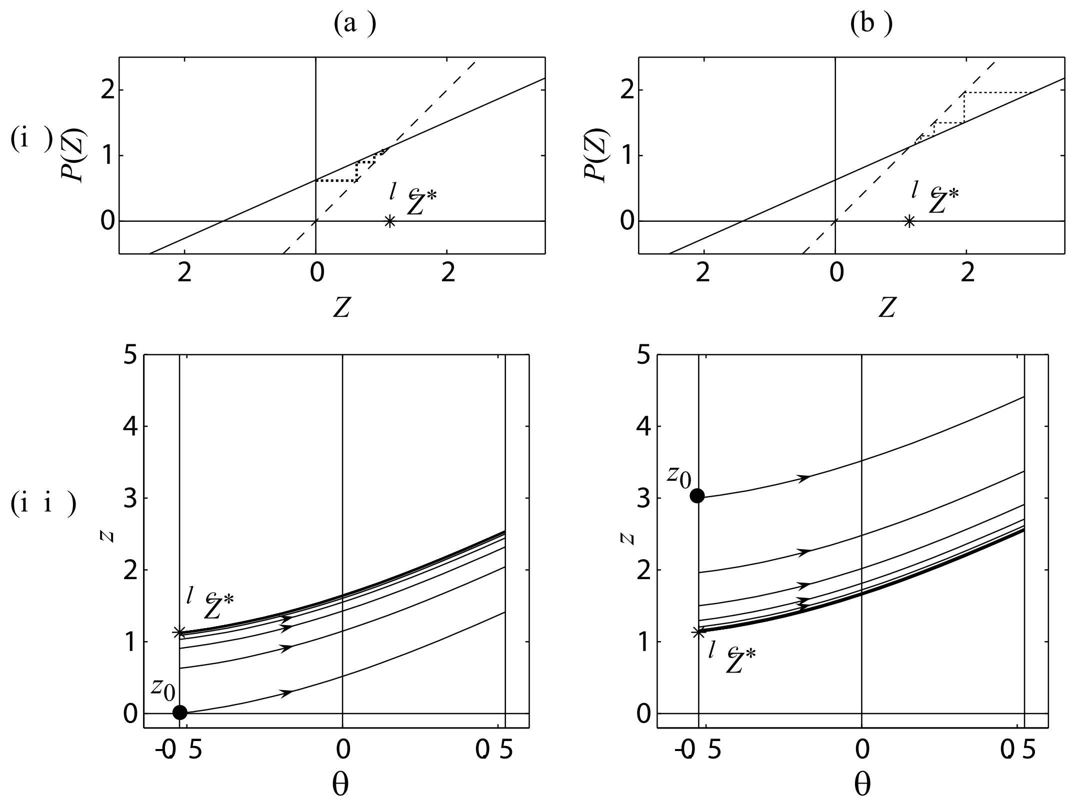

Figure 17: The plots shown here characterize behavior 1, Down$\xrightarrow{+}$ Limit Cycle. The wheel parameters are $\mu = \frac{2}{3}$, $n = 6$, and $\alpha = \frac{\pi}{4}$. The initial condition is $Z_0 = 0.0$. The fixed point is $^{lc}Z^* = 1.1313$. (b)The plots shown here characterize behavior 2, Down$\xrightarrow{-}$ Limit Cycle. The wheel parameters are $\mu = \frac{2}{3}$, $n = 6$, and $\alpha = \frac{\pi}{4}$. The initial condition is $Z_0 = 3.0$. The fixed point is $^{lc}Z^* = 1.1313$.

9 Energy Analysis

9.1 Approach to Fixed Points

How limit cycles or the stopped position are approached can be seen by considering the energy of the wheel. Below, we will consider this discussion more formally. In between spoke collisions, the kinetic energy gained by the wheel is proportional to the distance the center of mass falls and is a constant. The energy lost per collision is variable, however, and proportional to the wheel speed squared.

If the wheel starts off very slowly on a large enough slope, the energy lost per collision is much less than the energy gained between collisions so that the speed of the wheel increases with each collision. The loss in energy per collision, proportional to the speed squared, eventually catches up with, but cannot exceed, the constant gain in energy and the wheel approaches a steady speed.

If the same wheel starts off very fast on a large enough slope, the energy lost per collision is much more than the energy gained between collisions so that the wheel speed decreases with each collision. But the energy lost per collision in this case eventually diminishes to, but not below, the constant gain in energy, and the wheel approaches the same steady speed.

If the slope is not high enough, the energy loss per collision is greater than the energy gained between collisions so that the wheel speed decreases. In this case, however, the wheel eventually reaches a condition where its speed after collision is too low to carry it past the vertical and the wheel falls backward, eventually coming to rest. Once the wheel falls backward, there is no gain in energy, only losses, as the wheel rocks back and forth between two spokes.

The approach to a limit cycle or static equilibrium is monotonic; *i.e.*, the wheel does not alternate between slowing down and speeding up. In addition, the only case in which the wheel speed can increase without bound is when the number of spokes is infinity, which is the case of the rolling disk.

9.2 Energy Loss per Spoke Collision with the Ground

The energy loss during each spoke collision is equal to the change in kinetic energy during the collision since there is no change in potential energy; *i.e.*, no change in elevation of the center of mass occurs at collisions. The non-dimensional energy loss during collision i is

$$\Delta KE_i = KE_i^+ - KE_i^- = \frac{1-\mu^2}{2\mu^2}|Z|. \tag{47}$$

ΔKE_i is independent of slope angle.

The energy gained by the wheel in falling downhill between the collisions is equal to the loss in potential energy and is a constant for a given slope and number of spokes. The non-dimensional gain in potential energy between collisions is

$$\Delta PE = PE_i^- - PE_{i-1}^+ = KE_i^- = 2\sin\alpha\sin\frac{\pi}{n}. \tag{48}$$

The wheel enters into a limit cycle motion when the energy lost in each collision is balanced by the energy gained in falling between collisions when the wheel makes it past the vertical in the downhill direction; *i.e.*, when

$$\frac{1-\mu^2}{2\mu^2}Z^* = 2\sin\alpha\sin\frac{\pi}{n}. \tag{49}$$

Solving this equation for the limit cycle measure of angular velocity, we get the fixed point

$$^{lc}Z^* \equiv \frac{4\mu^2\sin\frac{\pi}{n}\sin\alpha}{1-\mu^2} > 0 \tag{50}$$

which agrees, of course, with the previous result in Equation (19).

The fractional change in energy loss per collision is given by

$$\frac{\Delta KE_i}{KE_i^-} = 1-\mu^2 \tag{51}$$

which is independent of slope and the angular velocity of the wheel after collision. So, when $\mu = 0$ all of the wheel energy is lost in collision and when $\mu = 1$, which only happens if the number of spokes equals infinity, no energy is lost in collision.

9.3 Energy Loss per Revolution of the Wheel

Next, we are interested in the energy lost per revolution of the wheel in the limit as the number of spokes n goes to infinity, for two cases: (1) when the wheel is not in a limit cycle but has enough energy to make it past the vertical in the downhill direction and (2) when the wheel is in a limit cycle.

9.3.1 Non-steady State Energy Accounting

At any given speed not at steady-state but where the measure of angular velocity after each collision i is great enough for the wheel to pass the vertical position, $Z_i > {}^{dn}Z$, the non-dimensional energy loss per revolution of an n-spoked wheel is

$$\xi = \frac{1-\mu^2}{4\mu^2 n \sin\frac{\pi}{n}} \sum_{i=1}^{n} |Z_i| = \frac{1-\mu^2}{4\mu^2 n \sin\frac{\pi}{n}} \sum_{i=1}^{n} P^i(Z_0), \tag{52}$$

where $Z_0 \neq {}^{lc}Z^*$ is the measure of angular velocity of the wheel just after the first collision in a particular revolution of the wheel, collision $i = 0$, and P is the return map. The energy loss per revolution has been further non-dimensionalized with respect to the perimeter Q_n of the rimless wheel (an equilateral polygon),

$$Q_n = 2n \sin\frac{\pi}{n}. \tag{53}$$

Iterating P under the summation in Equation (52), we obtain

$$\xi = \frac{1-\mu^2}{4\mu^2 n \sin\frac{\pi}{n}} \sum_{i=1}^{n} \left[\mu^{2i} Z_0 + 4\sin\alpha \sin\frac{\pi}{n} \sum_{r=1}^{i} \mu^{2r}\right] \tag{54}$$

Summing the two series and simplifying yields

$$\xi = \frac{1}{2}\left[\frac{Z_0(1-\mu^{2n})}{2n\sin\frac{\pi}{n}} + \frac{2\sin\alpha}{n}\left(n - \frac{(1-\mu^{2n})\mu^2}{1-\mu^2}\right)\right] \tag{55}$$

Expanding ξ from Equation (55) in an asymptotic series about $\frac{1}{n} = 0$, we find for large n that

$$\xi \approx \lambda^2(Z_0 + 2\sin\alpha)\frac{1}{n}. \tag{56}$$

Thus, as the number of spokes goes to infinity, the energy loss per revolution goes to zero and, as we will show subsequently, the average speed of the wheel approaches infinity, as for a disk with axisymmetric mass distribution.

9.3.2 Limit Cycle Energy Accounting

When the wheel is in a limit cycle, the measure of angular velocity after each collision in a revolution is $Z_i = {}^{lc}Z^*$ and the non-dimensional energy lost per revolution is

$$\xi^* = \frac{1-\mu^2}{4\mu^2} n \sin\frac{\pi}{n} \sum_{i=1}^{n} |Z_i| = \frac{1-\mu^2}{4\mu^2 n \sin\frac{\pi}{n}} n({}^{lc}Z^*)^2 = \sin\alpha. \tag{57}$$

At steady state, the non-dimensional energy loss per revolution simply equals the sine of the slope angle α for any number of spokes n. A graph of the non-dimensional energy loss per revolution ξ is shown as a function of revolution number in Figure 18(a). In addition, we show in Figure 18(b) a plot of the non-dimensionalized potential energy, kinetic energy, and total energy of the rimless wheel versus time for the case of the wheel approaching a limit cycle from above, the behavior denoted by Down$\bar{\rightarrow}$ Limit Cycle.

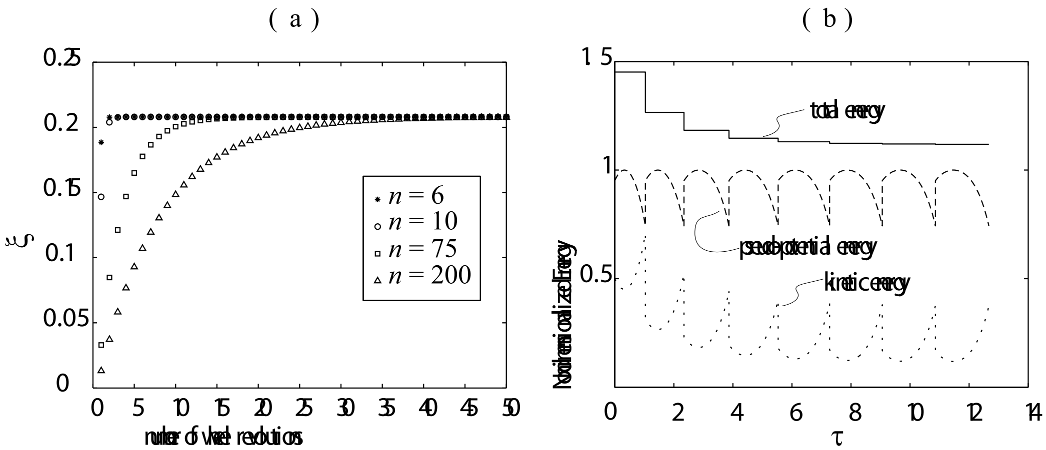

Figure 18: (a) Non-dimensionalized energy loss per revolution up to steady state for $\mu = \frac{2}{3}$, $\alpha = \frac{\pi}{15}$, and n = 6, 10, 75 and 200 spokes. After many revolutions, and, hence, many spoke collisions, the energy loss per revolution is $\xi^* = \sin\alpha = 0.2079$ as the wheel approaches a limit cycle, for any number of spokes n. (b) The non-dimensionalized potential energy, kinetic energy, and total energy of the rimless wheel are plotted versus time as the wheel approaches a limit cycle from above. The total energy is conserved between collisions but decreases with every collision due to the dissipative impact. The potential energy of the wheel between every collision is always measured with respect to a datum set at the foot of the spoke currently in contact with the ground. We thus term this unusual energy measure *pseudo-potential energy.* The range of the pseudo-potential energy is determined by the wheel parameters. Eventually, the total energy between collisions becomes constant as the wheel approaches a limit cycle motion. The energy lost per collision is represented by the vertical *dotted* lines and the energy gained between collisions, a constant, is represented by the vertical *dashed* lines. The plot shows that the wheel starts off at a speed greater than the limit cycle speed. Since the kinetic energy of the wheel is proportional to the wheel speed squared, at first the energy loss per collision is much greater than the energy gain between collisions so that the wheel speed decreases with each collision. The energy lost per collision eventually diminishes to, but not below, the constant gain in energy and the wheel speed after each collision converges to the limit cycle speed. As the wheel enters into the limit cycle, the vertical portions of the curves representing the energy loss at collisions and the energy gain between collisions approach the same length, indicating the eventual balance between energy loss and energy gain.

10 Average Speed and Average Rate of Change of Speed in the Limit Cycle

10.1 Limit Cycle Period

Let $\Delta\tau_{lc}$ be the non-dimensional time between spoke collisions in the limit cycle. From the first integral of motion in Equation (11), we obtain

$$\Delta\tau_{lc} = \int_{-\frac{\pi}{n}}^{\frac{\pi}{n}} \frac{d\theta}{\sqrt{({}^{lc}\dot{\theta}^*)^2 + 2(\cos(\alpha - \frac{\pi}{n}) - \cos(\alpha + \theta))}} \tag{58}$$

10.2 Average Speed of the Center of Mass

The non-dimensional speed of the center of mass in between collisions for downhill rolling is

$$v_{cm}(\tau) = \dot{\theta}(\tau) \tag{59}$$

where we have non-dimensionalized the speed with respect to the spoke length ℓ. The non-dimensionalized average speed of the center of mass in the limit cycle is

$$v_{cm_{avg}} = \frac{1}{\Delta\tau_{lc}} \int_0^{\Delta\tau_{lc}} \left|\frac{d\theta(\tau)}{d\tau}\right| d\tau = \frac{1}{\Delta\tau_{lc}} \theta(\tau)|_0^{\Delta\tau_{lc}} = \frac{1}{\Delta\tau_{lc}} \left[(\frac{\pi}{n}) - (-\frac{\pi}{n})\right] = \frac{1}{\Delta\tau_{lc}} \frac{2\pi}{n}. \quad (60)$$

Figure 19(a) shows the non-dimensionalized average speed of the rimless wheel in the limit cycle plotted as a function of slope angle for a variety of number of spokes.

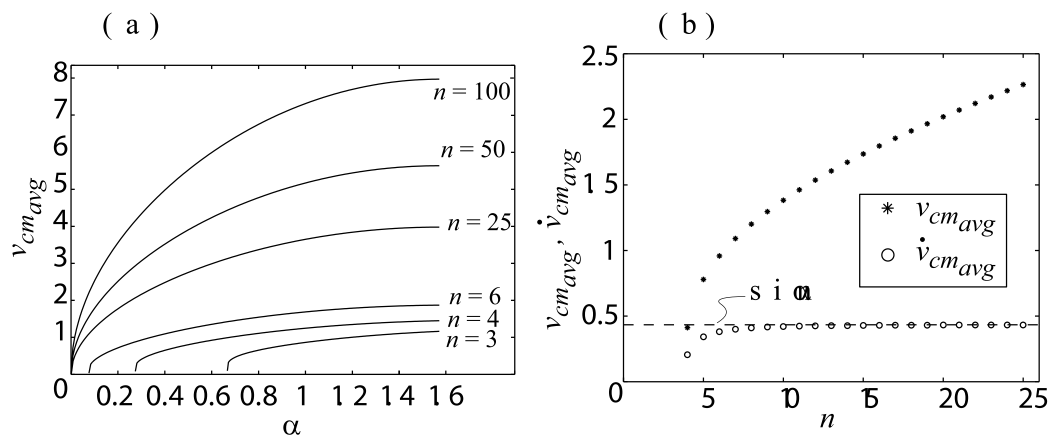

Figure 19: (a) Non-dimensionalized average speed at steady state, $v_{cm_{avg}}$, as a function of slope angle with $\alpha_c < \alpha < \frac{\pi}{2}$ and for $n = 3$, 4, 6, 25, 50, and 100 spokes. As expected, the steady state speed increases with the number of spokes and slope angle. (b) Non-Dimensionalized average speed, $v_{cm_{avg}}$, and average rate of change of speed, $\dot{v}_{cm_{avg}}$, of the rimless wheel at steady state as a function of number of spokes $n = 4$ to $n = 25$ spokes and fixed slope angle $\alpha = \frac{\pi}{7}$. As the number of spokes gets large, the speed increases without bound and the rate of change of speed is asymptotic to $\dot{v}_{cm_{avg}} = \sin\alpha = 0.4339$, indicated by the horizontal dashed line which is the acceleration of a disk of any axisymmetric mass distribution (non-dimensionalized by its moment of inertia) rolling down a slope of angle α. The plot shows that, for finite slope angle, the average speed is proportional to $n^{\frac{1}{2}}$, even for fairly small numbers of spokes.

10.3 Average Rate of Change of Speed

The non-dimensionalized average rate of change of speed of the center of mass in the limit cycle is

$$\dot{v}_{cm_{avg}} = \frac{1}{\Delta\tau_{lc}} \int_0^{\Delta\tau_{lc}} \left|\frac{d\dot{\theta}(\tau)}{d\tau}\right| d\tau = \frac{1}{\Delta\tau_{lc}} \dot{\theta}(\tau)|_0^{\Delta\tau_{lc}} = \frac{1}{\Delta\tau_{lc}} [\frac{{}^{lc}\dot{\theta}^*}{\mu} - {}^{lc}\dot{\theta}^*] = \frac{1}{\Delta\tau_{lc}} \frac{1-\mu}{\mu} ({}^{lc}\dot{\theta}^*). \quad (61)$$

10.4 Asymptotic Behavior for Large n

In the limit as the number of spokes goes to infinity, we expect the rimless wheel to behave like a disk with an axisymmetric mass distribution rolling down a slope without slip or frictional losses; *i.e.*, the limit cycle period should go to zero, the average limit cycle speed of the center of mass to infinity, and the rate of change of speed of the center of mass to a constant. To check, we first compute the non-dimensional time between collisions for finite slope angle as n gets large. To do this, we assume that the integrand becomes nearly constant as the interval $[-\frac{\pi}{n}, \frac{\pi}{n}]$ shrinks to zero:

$$\Delta\tau_{lc} = \int_{-\frac{\pi}{n}}^{\frac{\pi}{n}} \frac{d\theta}{\sqrt{({}^{lc}\dot{\theta}^*)^2 + 2(\cos(\alpha - \frac{\pi}{n}) - \cos(\alpha + \theta)}}$$

$$\approx \quad \frac{1}{\sqrt{({}^{lc}\dot{\theta}^*)^2 + 4\sin\alpha\sin\frac{\pi}{n}}} \int_{-\frac{\pi}{n}}^{\frac{\pi}{n}} d\theta = \frac{\pi}{n}\sqrt{\frac{1-(1+\lambda^2(\cos(\frac{2\pi}{n})-1))^2}{\sin\alpha\sin\frac{\pi}{n}}}. \tag{62}$$

where, to recall, $\lambda^2 = \frac{1}{\frac{I_C}{m\ell^2}+1}$.

Expanding the approximate limit cycle time from Equation (62) in an asymptotic series about $\frac{1}{n} = 0$, we find for large n that

$$\Delta\tau_{lc} \approx 2\left(\frac{\lambda^2}{\sin\alpha}\right)^{\frac{1}{2}}\left(\frac{\pi}{n}\right)^{\frac{3}{2}}. \tag{63}$$

Thus, as the number of spokes goes to infinity, the average limit cycle time does shrink to zero.

Referring to Equation (62), the average speed in the limit cycle for large n is thus

$$v_{cm_{avg}} = \frac{1}{\Delta\tau_{lc}}\frac{2\pi}{n} \approx 2\sqrt{\frac{\sin\alpha\sin\frac{\pi}{n}}{1-(1+\lambda^2(\cos(\frac{2\pi}{n})-1))^2}}. \tag{64}$$

Expanding the approximate average speed from Equation (64) in an asymptotic series about $\frac{1}{n} = 0$, we find for large n that

$$v_{cm_{avg}} \approx \left(\frac{\sin\alpha}{\lambda^2}\right)^{\frac{1}{2}}\left(\frac{\pi}{n}\right)^{-\frac{1}{2}}. \tag{65}$$

Thus, as the number of spokes goes to infinity, the average limit cycle speed does go to infinity.

For the average rate of change of speed in the limit cycle approximated for large n, we have

$$\dot{v}_{cm_{avg}} = \frac{1}{\Delta\tau_{lc}}\frac{1-\mu}{\mu}({}^{lc}\dot{\theta}^*) \approx \frac{\sin\alpha\sin\frac{\pi}{n}}{\frac{\pi}{n}}\frac{2}{2+\lambda^2(\cos\frac{2\pi}{n}-1)}. \tag{66}$$

In this case, as $n \to \infty$, we can see simply by inspection that $\dot{v}_{cm_{avg}} \to \sin\alpha$. Also, we can expand the approximate average rate of change of speed from Equation (66) in an asymptotic series about $\frac{1}{n} = 0$ to see how it varies with n

$$\dot{v}_{cm_{avg}} \approx \sin\alpha\left(1+\left(\frac{\pi}{n}\right)^2\left(\lambda^2-\frac{1}{6}\right)\right). \tag{67}$$

As the number of spokes gets large, then, the speed and acceleration of the center of mass of the rimless wheel in the limit cycle become that of a disk rolling down a slope of angle α. Figure 19(b) displays this behavior.

Small Slope Angle α

For small slope angle, $\sin\alpha \approx \alpha$. To make a more useful approximation for small α, however, based on a large number number of spokes, we make use of the following observation. For large n, we find from Equation (22) that the critical angle for the existence of limit cycles is $\alpha_c \sim O\left(\frac{1}{n^3}\right)$. We take α to be small as well as let n get large, say, $\alpha \sim O(\frac{1}{n})$ (so that it is still bigger than α_c for large n, guaranteeing the existence of limit cycles). In this approximation, the slope angle is on the order of β, the angle between the spokes. We find, then, that $\Delta\tau_{lc}$ (limit cycle period), $\dot{v}_{cm_{avg}}$ (limit cycle average rate of change of speed), and ξ^* (energy lost per revolution in a limit cycle) are all $\sim O(\frac{1}{n})$. The limit cycle average speed, however, is $v_{cm_{avg}} \sim O(1)$. Thus, for $\alpha \sim O(\frac{1}{n})$, as the number of spokes goes to infinity, the slope angle and the angle between spokes go to zero at the same rate. As a result, the rate of change of speed and energy lost per revolution in a limit cycle go to zero as well. The limit cycle average speed, however, goes to a constant, as it should, since (for the particular case $\alpha \sim O(\frac{1}{n})$), as the number of spokes goes to infinity the rimless wheel in a limit cycle becomes a disk rolling on level ground, not accelerated by gravity.

11 Conclusion

In this paper, we have extended McGeer's linear analysis for downhill rolling of the 2D rimless wheel to include the full nonlinear analysis and uphill rolling. In our analysis, we have defined a cycle of motion of the wheel, derived the equations of motion and collision transition conditions, defined the phase space of the motion, defined a Poincaré section and return map to represent the cyclic motion of the wheel, found the fixed points of the map that correspond to limit cycle motion and eventual stopping of the wheel, showed that the two fixed points are stable, and defined various behaviors of the wheel. In addition, we showed for what slope angles the fixed points and behaviors exist and carefully determined the basins of attraction for the fixed points in the intermediate slope angle regime. Analyses of the energy and speed of the wheel show that the wheel behaves like a disk rolling down a slope when the number of spokes is infinity. The results, though expansive, add only a little depth to McGeer's results which capture the wheel's essential behavior - that it can have stable periodic motions. For small slope angles and large numbers of spokes, all of the results of the nonlinear analysis reduce to the results of McGeer's linear analysis.

Acknowledgments

The authors thank Daniel Koditschek for his discussions on the phase surface for the wheel; Anindya Chatterjee for showing how to evaluate the integral for the limit cycle period for large numbers of spokes; Rudra Pratap for his help with writing MATLAB® integration routines that detect collisions; and, Dave Cabrera for his careful editing of the paper.

References

[1] A. A. Andronov, A. A. Vitt, and S. E. Khaikin. *Theory of Oscillators.* Dover, 1966.

[2] M. Coleman, A. Chatterjee, and A. Ruina. Motions of a rimless spoked wheel: A simple 3D system with impacts. *Dynamics and Stability of Systems*, 12(3):139–69, September 1997.

[3] Rodolfo Margaria. *Biomechanics and Energetics of Muscular Excercise.* Clarendon Press, Oxford, 1976.

[4] T. McGeer. Stability and control of two-dimensional biped walking. Technical Report CSS-IS TR 88-01, Simon Fraser University Centre for Systems Science, Burnaby, B.C., Can., September 1988.

[5] T. McGeer. Powered flight, child's play, silly wheels, and walking machines. In *Proc., IEEE International Conference on Robotics and Automation*, pages 1592–7, Piscataway, NJ, 1989. IEEE, IEEE.

[6] T. McGeer. Passive dynamic walking. *Int. J. Robot. Res.*, 9(2):62–82, April 1990.

[7] T. McGeer. Passive walking with knees. In *Proc., 1990 IEEE International Conference on Robotics and Automation*, pages 1640–5, Los Alamitos, CA, 1990. IEEE, IEEE.

[8] T. McGeer. Passive dynamic biped catalogue. In R. Chatila and G. Hirzinger, editors, *Proc., Experimental Robotics II: The 2nd International Symposium*, pages 465–90, Berlin, 1992. Springer–Verlag.

[9] T. McGeer and L. H. Palmer. Wobbling, toppling, and forces of contact. *American Journal of Physics*, 57:1089–96, December 1989.